Forschungszentrum Karlsruhe
Technik und Umwelt

Wissenschaftliche Berichte

FZKA 6104

Stellar Neutron Capture Cross Sections of Pr and Dy Isotopes

F. Voss, K. Wisshak, F. Käppeler, L. Kazakov

Institut für Kernphysik

Mai 1998

FORSCHUNGSZENTRUM KARLSRUHE

Technik und Umwelt

Wissenschaftliche Berichte

FZKA 6104

STELLAR NEUTRON CAPTURE CROSS SECTIONS OF Pr AND Dy ISOTOPES

F. VOSS, K. WISSHAK, F. KÄPPELER, and L. KAZAKOV[1]

Institut für Kernphysik

[1]Institute for Physics and Power Engineering, Obninsk-Kaluga Region, Russia

Forschungszentrum Karlsruhe GmbH, Karlsruhe
1998

Als Manuskript gedruckt

Forschungszentrum Karlsruhe GmbH
Postfach 3640, 76021 Karlsruhe

Mitglied der Hermann von Helmholtz-Gemeinschaft
Deutscher Forschungszentren (HGF)

ISSN 0947-8620

ABSTRACT

The neutron capture cross sections of ^{160}Dy, ^{161}Dy, ^{162}Dy, ^{163}Dy, ^{164}Dy, and ^{141}Pr have been measured in the energy range from 3 to 225 keV at the Karlsruhe 3.75 MV Van de Graaff accelerator. Neutrons were produced via the ^{7}Li$(p,n)^{7}$Be reaction by bombarding metallic Li targets with a pulsed proton beam. Capture events were registered with the Karlsruhe 4π Barium Fluoride Detector. The cross sections were determined relative to the gold standard. For the first time the correction for undetected capture events was completely obtained from experimental information, using capture cascades derived from measurements with an ADC system. The cross section ratios could be determined with an overall uncertainty of 1–1.5%, an average improvement compared to previous measurements by a factor 4.

Maxwellian averaged neutron capture cross sections were calculated for thermal energies between kT = 10 keV and 100 keV. For most of the isotopes there is reasonable agreement with recent evaluations, but discrepancies of ~20% were obtained for ^{160}Dy and ^{164}Dy.

ZUSAMMENFASSUNG

DIE STELLAREN (n,γ) QUERSCHNITTE DER Pr UND Dy ISOTOPE

Die Neutroneneinfangquerschnitte von ^{160}Dy, ^{161}Dy, ^{162}Dy, ^{163}Dy, ^{164}Dy und ^{141}Pr wurden im Energiebereich von 3 bis 225 keV am Karlsruher Van de Graaff Beschleuniger relativ zu Gold als Standard bestimmt. Neutronen wurden über die ^{7}Li(p,n)^{7}Be–Reaktion durch Beschuß metallischer Li–Targets mit einem gepulsten Protonenstrahl erzeugt. Der Nachweis von Einfangereignissen mit dem Karlsruher 4π Barium Fluorid Detektor konnte erstmals vollständig auf der Grundlage experimenteller Informationen geführt werden, da sich die Korrektur für nicht beobachtete Ereignisse aus den mit einem ADC System gemessenen Einfangkaskaden bestimmen ließ. Die Querschnittsverhältnisse sind mit einer Unsicherheit von 1–1.5% im Mittel um einen Faktor 4 genauer als frühere Ergebnisse.

Die stellaren Einfangquerschnitte wurden für thermische Energien von kT = 10 keV bis 100 keV berechnet. Für die meisten Isotope gibt es eine gute Übereinstimmung mit den Werten neuerer Evaluationen, für ^{160}Dy und ^{164}Dy wurden allerdings Abweichungen bis zu 20% gefunden.

Contents

1 INTRODUCTION

The present measurement of the (n,γ) cross sections of ^{141}Pr and a series of dysprosium isotopes is part of a comprehensive study of the rare earth region with the Karlsruhe 4πBaF$_2$ detector [1, 2, 3]. This project is motivated by the need for an accurate data basis to study the nucleosynthesis of the heavy elements in the slow neutron capture process (s process). The rare earth region is of special importance in this respect since the solar abundances of this chemically almost identical elements is very well known [4]. Thus the most important quantity in these studies, the product of s–process abundance and stellar capture cross section, $N_s\langle\sigma\rangle$, can be reliably determined for a wide mass range.

The s–process path in the region of dysprosium is sketched in Fig. 1. The s–only isotope ^{160}Dy is shielded by its stable Gd isobar from contributions of the r process and is only marginally affected by a weak branching at ^{160}Tb. It therefore represents an important normalization point of the $N_s\langle\sigma\rangle$–systematics. Any deviation of the empirical $N_s\langle\sigma\rangle$–product from the systematics, which is well defined in the rare earth region would indicate a thermal enhancement of the capture cross section under the high s–process temperatures. Theoretical estimates by Harris [5] and Holmes *et al.* [6] predict, indeed, an effect of about 10% at 30 keV.

The isotope ^{163}Dy is one of the exotic cases, where a terrestrially stable isotope starts to decay in the stellar s–process environment due to the almost complete ionization. The responsible mechanism is the emission of decay electrons into the unoccupied atomic orbits, thereby enhancing the decay Q-value by the respective electron binding energy. This bound state β–decay [7] was successfully verified for the example of ^{163}Dy in a recent experiment [8]. As shown in Fig. 1 this behavior results in a branching of the reaction path at ^{163}Dy leading to the production of the s–only isotope ^{164}Er. The strength of this branching, which has been recently studied in detail [9], depends partly on the capture cross section of ^{163}Dy.

The capture cross sections of all dysprosium isotopes are required for defining the s–process abundance pattern for comparison with the expected isotopic anomalies in meteoritic inclusions. A first hint of an anomalous Dy sequence, which is very difficult to observe, has been reported by Richter *et al.* [10].

The dysprosium isotopes are located at the position of an intermediate peak in the r–process abundance distribution at A = 163, which can be used to constrain the conditions under which the r–process freezes out [11]. Since the r distribution is obtained as the difference between solar and s–process abundances a reliable correction for the s–process part is important, even though the solar abundances are dominated by the r process.

The isotope ^{141}Pr was investigated in order to complete a recent study of the Ce/Pr/Nd region [3], where it constitutes part of a weak branching bypassing the s–only nucleus ^{142}Nd.

Previous studies of the investigated isotopes show reasonably good agreement on the

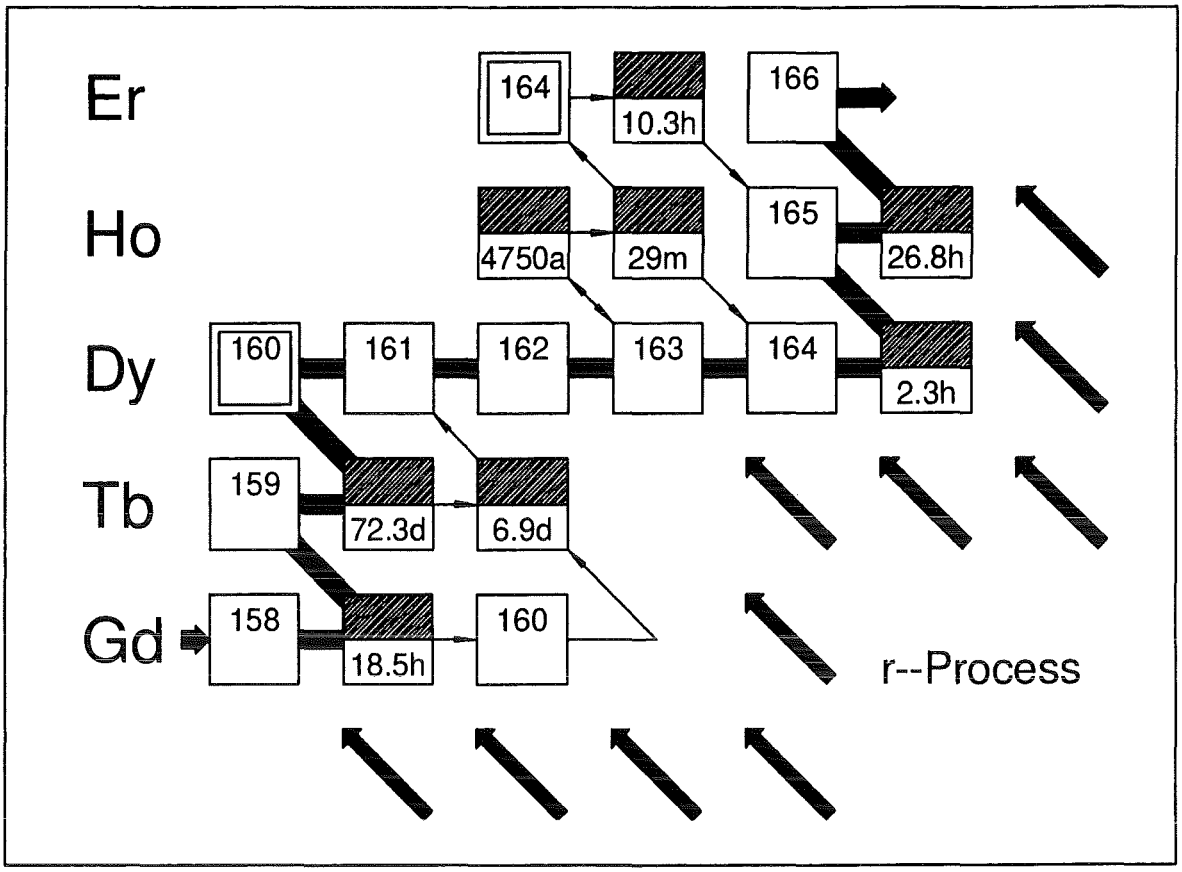

Figure 1: The reaction path of the s process in the region of the dysprosium isotopes.

$\pm 10\%$ level corresponding to the uncertainties of these data, but discrepancies of 30% were reported for ^{160}Dy and ^{162}Dy.

With the present experiment it is intended to resolve the existing discrepancies of the stellar (n,γ) cross sections of praseodymium and of the dysprosium isotopes and to establish a significantly improved data basis for detailed s-process analyses. The measurements and data analyses are described in Secs. 2 and 3, followed by a discussion of the results and uncertainties in Secs. 4 and 5. The stellar cross sections are presented in Sec. 6. The astrophysical implications will be addressed in a forthcoming publication.

2 EXPERIMENT

2.1 Experimental Method

The neutron capture cross sections of ^{141}Pr and the dysprosium isotopes 160 to 164 have been measured in the energy range from 3 to 225 keV using gold as a standard. Since the experimental method has been published in detail [1, 12, 13, 14], only a general description is given here, complemented with the specific features of the present measurement.

Neutrons were produced via the ^{7}Li$(p,n)^{7}$Be reaction by bombarding metallic Li targets with the pulsed proton beam of the Karlsruhe 3.75 MV Van de Graaff accelerator. The neutron energy was determined by time of flight (TOF), the samples being located at a flight path of 79 cm. The relevant parameters of the accelerator were a pulse width of <1 ns, a repetition rate of 250 kHz, and an average beam current of 2.0 μA. In different runs, the proton energies were adjusted 30 and 100 keV above the threshold of the ^{7}Li$(p,n)^{7}$Be reaction at 1.881 MeV. In this way, continuous neutron spectra in the proper energy range for s–process studies were obtained, ranging from 3 to 100 keV, and 3 to 225 keV, respectively. The lower maximum neutron energy offers a significantly better signal to background ratio at lower energies.

Capture events were registered with the Karlsruhe 4π Barium Fluoride Detector via the prompt capture γ–ray cascades. This detector consists of 42 hexagonal and pentagonal crystals forming a spherical shell of BaF_2 with 10 cm inner radius and 15 cm thickness. It is characterized by a resolution in γ–ray energy of 7% at 2.5 MeV, a time resolution of 500 ps, and a peak efficiency of 90% at 1 MeV. The 1.6 MeV threshold in γ–ray energy corresponds to an efficiency for capture events of more than 98% for all investigated isotopes. A comprehensive description of this detector can be found in Ref. [13].

The experiment was divided into three runs, two using the conventional data acquisition technique with the detector operated as a calorimeter, and one with an ADC system coupled to the detector for analyzing the signals from all modules individually. In this way, the full spectroscopic information recorded by the detector can be recovered.

2.2 Samples

The dysprosium samples were prepared from isotopically enriched oxyde powder (Dy_2O_3) which was heated to 1200 K for 15 min to eliminate any water contaminations. Then the various batches were pulverized in an agate mortar, pressed into pellets of 15 mm diameter, and reheated to 1200 K for 1 hour. During the final heating the pellets shrinked slightly. Immediately after cooling, the actual samples were prepared by canning the pellets into air tight aluminum cylinders with 0.2 mm thick walls. In the first heating step the various batches of enriched isotopes lost between 0.1% and 4.3% in weight, whereas no further losses could be observed in the second step.

The praseodymium sample was prepared in the same way, but was more difficult to characterize since the oxyde of this element has no well defined stoichiometry. The mix-

ture of the praseodymium (III,IV) oxide is generally specified as Pr_6O_{11} ($PrO_{1.83}$), but the exact oxygen content could not be specified by the supplier. Therefore, the stoichiometry was experimentally determined by K–edge densiometry [15, 16] as described in Ref. [1]. Part of the praesodymium powder used for the preparation of the sample was dissolved in nitric acid and diluted to a concentration of ~30 mg/ml. The exact praseodymium content was determined by observing the X–ray absorption in the region of the K–edge. The measurement was calibrated by means of three standard solutions of about the same concentration prepared from praseodymium metal which was carefully handled under argon atmosphere. The measured stoichiometry was found to be $PrO_{1.94}$. Compared to the standard value this corresponds to a one percent difference in the calculated praseodymium mass.

When the canned samples were controlled after the experiment, the weight had increased by 0.06% on average. At least to some extent, this increase is due to the glue which was used to fix the samples in the sample ladder and which could not be removed completely. Thus, any significant water contamination during the experiment could be excluded.

In addition to the praseodymium and the 5 dysprosium samples, a gold sample in an identical Al canning was used for measuring the neutron flux. An empty canning was mounted on the sample ladder for determining the sample independent background.

A ^{208}Pb sample and a graphite sample served for simulating the background due to scattered neutrons in order to study whether the slightly different energy losses in the scattering process and the related TOF shifts of the scattered neutrons may affect this correction. In the first run of the experiment both scattering samples were mounted simultaneously, thus allowing a direct check whether the evaluated cross sections depend on the scattering sample used for correction. In the other runs the ^{208}Pb sample was replaced by the ^{141}Pr sample.

The relevant sample parameters are compiled in Table 1, and the isotopic composition of the dysprosium samples provided by the supplier (IPPE Obninsk) is listed in Table 2.

The neutron transmission of the samples calculated with the SESH code [17] was generally larger than 90% (Table 3). The measured spectra of all samples were normalized to equal neutron flux by means of a ^6Li–glass monitor located close to the neutron target. The transmission spectra measured with a second ^6Li–glass detector at a flight path of 260 cm were used for a rough determination of the total cross sections. Though the accuracy of this method is inferior to that obtained in a dedicated experiment, these total cross sections can be used to test the normalization to equal neutron flux (Sec. 3). Before the third run the lithium glass of this detector (diameter 39 mm, thickness 3 mm) was replaced by a new one (diameter 30 mm, thickness 4 mm). While the old scintillator was almost exactly shaded by the sample, thus requiring very accurate adjustment, this problem is more relaxed with the new scintillator.

Table 1: SAMPLE CHARACTERISTICS

Sample	Diameter	Thickness		Weight[a]	Canning[b]	Neutron binding
	(mm)	(mm)	(10^{-3}at/barn)[c]	(g)	(g)	energy (MeV)
^{164}Dy	14.7	5.2	7.2455	3.9946	0.2476	5.716
Graphite	15.0	2.5	21.688	0.7644	0.2136	
^{161}Dy	14.1	0.9	0.9789	0.5317	0.1780	8.197
^{160}Dy	14.9	2.2	3.3794	1.8333	0.2070	6.454
^{197}Au	15.0	0.4	2.2475	1.2990	0.1849	6.513
^{163}Dy	14.8	1.2	1.8737	1.0285	0.2025	7.658
^{141}Pr[d]	14.9	4.2	5.6363	2.8431	0.2519	5.844
Empty					0.1810	
^{162}Dy	14.9	2.8	3.9286	2.1468	0.2220	6.271
^{208}Pb[e]	15.0	1.9	5.7243	3.4933	0.1820	

[a]For dysprosium samples: weight of Dy_2O_3
For praseodymium sample: weight of $PrO_{1.94}$ (see text)
[b]Aluminum cylinder
[c]For dysprosium samples: sum of all Dy isotopes
[d]Used in Runs II and III
[e]Used in Run I

Table 2: ISOTOPIC COMPOSITION (%)

Sample	Isotope				
	^{160}Dy	^{161}Dy	^{162}Dy	^{163}Dy	^{164}Dy
^{160}Dy	42.4	37.4	13.4	4.5	2.3
^{161}Dy	6.9	80.8	8.8	2.4	1.1
^{162}Dy	0.2	1.0	92.4	5.6	0.8
^{163}Dy	0.0	0.3	1.8	89.9	8.0
^{164}Dy	0.1	0.5	1.2	7.4	90.8

2.3 Measurements

The samples were moved cyclically into the measuring position by a computer controlled sample changer. The data acquisition time per sample was about 10 min, a complete cycle lasting about 1.5 h. From each event, a 64 bit word was recorded on DAT tape containing the sum energy and TOF information together with 42 bits identifying those detector modules that contributed. Overall, 49 Gbyte of data were stored on tape. The relevant parameters of the three runs which were carried out with neutron spectra of different maximum energies are listed in Table 4. The data in Run III were recorded with the ADC system.

Table 3: CALCULATED NEUTRON TRANSMISSION[a]

Sample	Neutron Energy (keV)				
	10	20	40	80	160
^{197}Au	0.959	0.965	0.970	0.974	0.979
^{160}Dy	0.934	0.941	0.946	0.950	0.955
^{161}Dy	0.979	0.982	0.983	0.985	0.986
^{162}Dy	0.928	0.934	0.938	0.943	0.947
^{163}Dy	0.963	0.967	0.970	0.973	0.976
^{164}Dy	0.880	0.887	0.894	0.900	0.907
^{141}Pr	0.915	0.922	0.929	0.934	0.939

[a] Monte Carlo calculation with SESH code [17].

Table 4: PARAMETERS OF THE INDIVIDUAL RUNS

Run	Flight Path (mm)	TOF Scale (ns/ch)	Number of Cycles	Maximum Neutron Energy (keV)	Measuring Time (d)	Mode of Operation	Average Beam Current (μA)	Threshold in Sum Energy (MeV)
I	787.3	0.7603	245	100	15.7	Calorimeter	2.0	1.8
II	787.6	0.7602	251	200	15.3	Calorimeter	2.0	1.5
III	787.4	0.7092	297	100	18.6	ADC	1.9	1.6

3 DATA ANALYSIS

3.1 Total Cross Sections

The total cross sections of the investigated isotopes were determined in the neutron energy range from 10 to 200 keV via the TOF spectra measured with the ^{6}Li glass detector at a flight path of 260 cm. The total cross sections and the related uncertainties were obtained as described in Ref. [1], and are listed in Table 5. The results deduced for the carbon sample agree with the data from the Joint Evaluated File (JEF) [18] within $\pm$4.4%, similar to the measurements reported in Refs. [1, 19]. The quoted uncertainties were obtained under the assumption that they are inversely proportional to the fraction of neutrons interacting in the sample, A=1-T, where T is the transmission. For the carbon sample this fraction is A=8.8%, the related uncertainty of 4.4% being estimated from the comparison with the JEF data. The oxygen cross section was adopted from the JEF evaluation and its uncertainty was neglected. According to the above relation, the uncertainty was entirely ascribed to the respective dysprosium isotope. The total cross section determined for the ^{208}Pb sample is in good agreement with the data in Refs. [20, 21]. The combined cross section for elemental dysprosium was calculated neglecting

the rare isotopes ^{156}Dy and ^{158}Dy. These results as well as the total cross section of ^{141}Pr are in good agreement with the data given in Ref. [22].

Table 5: MEASURED TOTAL CROSS SECTIONS [a]

Neutron Energy	Total Cross Section (barn)								
(keV)	^{160}Dy	^{161}Dy	^{162}Dy	^{163}Dy	^{164}Dy	^{141}Pr	^{208}Pb	^{12}C	^{197}Au
10 – 15	8.8	17.9	13.1	13.7	11.2	6.1	10.4	4.36	15.6
15 – 20	12.3	15.7	12.4	14.0	11.4	7.0	10.3	4.47	13.2
20 – 30	9.4	14.9	12.1	10.9	11.0	6.9	10.7	4.43	13.1
30 – 40	6.9	15.9	11.4	11.9	9.8	6.5	10.3	4.34	12.4
40 – 60	10.1	11.5	10.7	10.2	9.9	5.3	10.3	4.33	11.5
60 – 80	9.1	11.5	9.8	9.0	9.6	5.1	13.7	4.29	10.5
80 – 100	9.1	10.1	9.9	8.8	8.3	5.0	10.5	4.20	10.5
100 – 150	7.6	10.0	8.9	7.6	8.6	4.7	–	4.20	8.5
150 – 200	7.6	8.7	9.0	6.9	8.2	4.8	–	4.00	7.5
Typical Uncertainty (%)	9.8	26	8.8	18	5.3	12	9.0	4.4	14

[a] Determined from the count rate of the ^{6}Li glass neutron monitor at 260 cm flight path

3.2 Capture Cross Sections

The analysis was carried out in the same way as described previously [1, 12, 14]. All events were sorted into two-dimensional spectra containing 128 sum energy versus 2048 TOF channels according to various event multiplicities (Evaluation 1). In Evaluation 2, this procedure was repeated by rejecting those events, where only neighboring detector modules contributed to the sum energy signal. With this option, background from the natural radioactivity of the BaF_2 crystals and from scattered neutrons can be reduced. For all samples, the resulting spectra were normalized to equal neutron flux using the count rate of the ^{6}Li glass monitor close to the neutron target. The corresponding normalization factors are below 0.4% for all runs. The treatment of the two-dimensional spectra from the data recorded with the ADC system is slightly more complicated and was performed as described in Ref. [1].

In the next step of data analysis, sample-independent backgrounds were removed by subtracting spectra measured with the empty canning. A remaining constant background was determined at very long flight times, where no time-correlated events are expected. The resulting two-dimensional spectra for events with multiplicity >2 measured in Run III are shown for all investigated isotopes in Figs. 2, 3, and 4. The TOF is plotted on the X-axis and the sum-energy on the Y-axis. Note that events with low sum-energy and large TOF are suppressed by the preprocessing in the ADC-system.

At this point, the spectra contain only events correlated with the sample. The next correction to be made is for isotopic impurities (see Ref.[1] for details). The respective coefficients are compiled in Table 6.

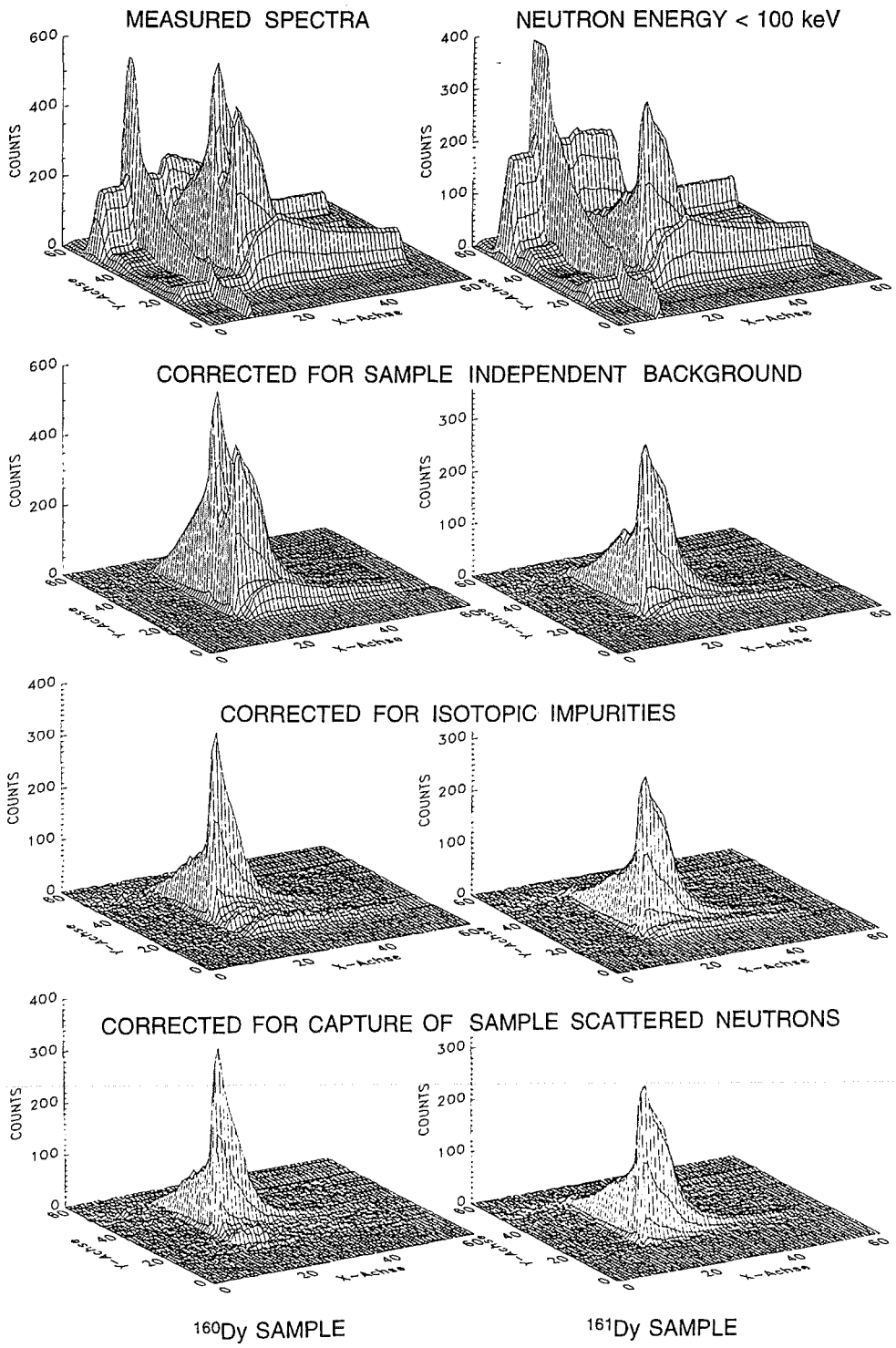

Figure 2: The different steps of background subtraction in the two-dimensional sum energy $\times$ TOF spectra. The data are shown for ^{160}Dy and ^{161}Dy measured in Run III with 100 keV maximum neutron energy and an event multiplicity >2. (The original resolution of 128 $\times$ 2048 channels was compressed into 64 $\times$ 64 channels for better readability. The TOF is plotted on the X-axis and the sum-energy on the Y-axis).

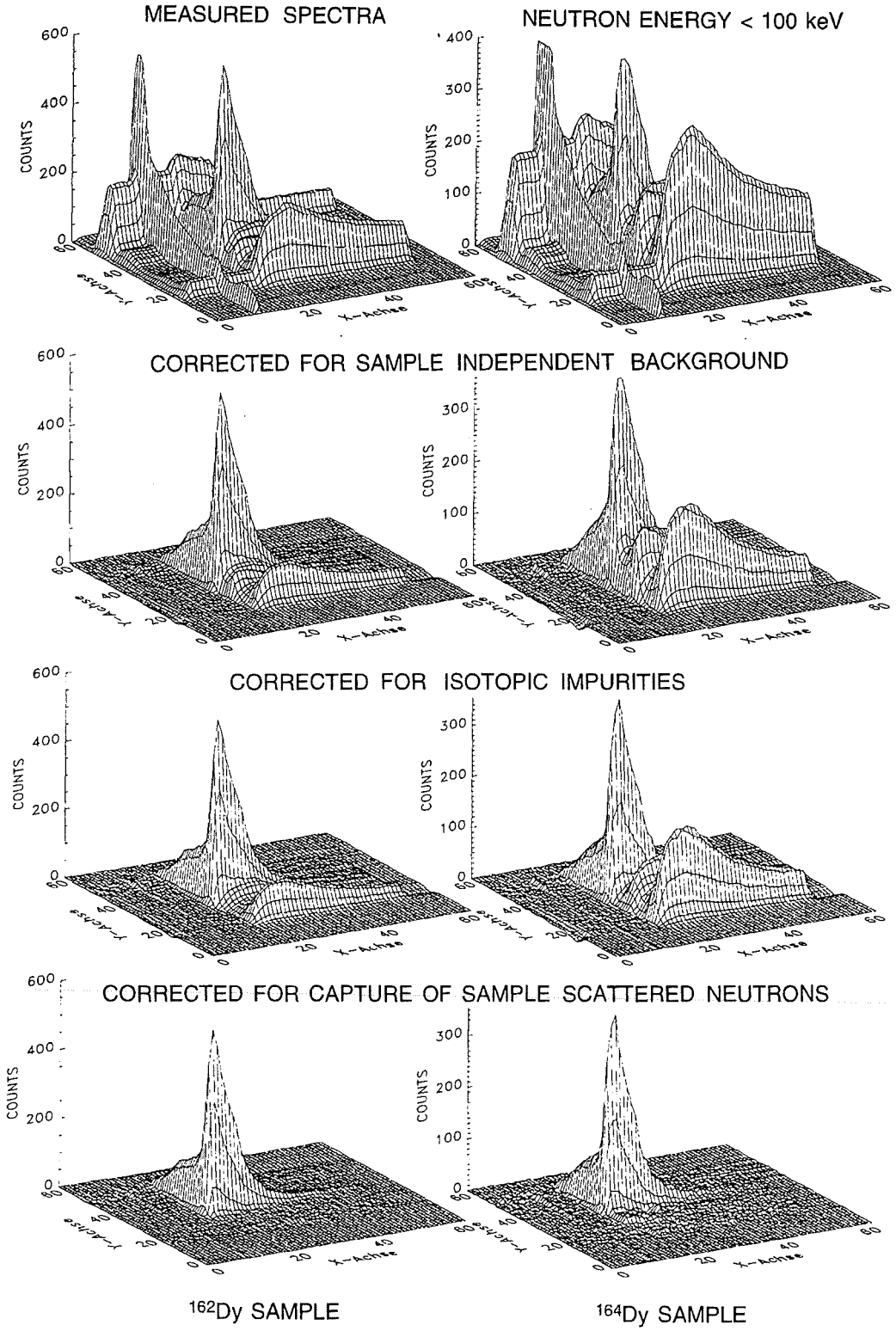

Figure 3: As Fig. 2 but for the ^{162}Dy and ^{164}Dy samples.

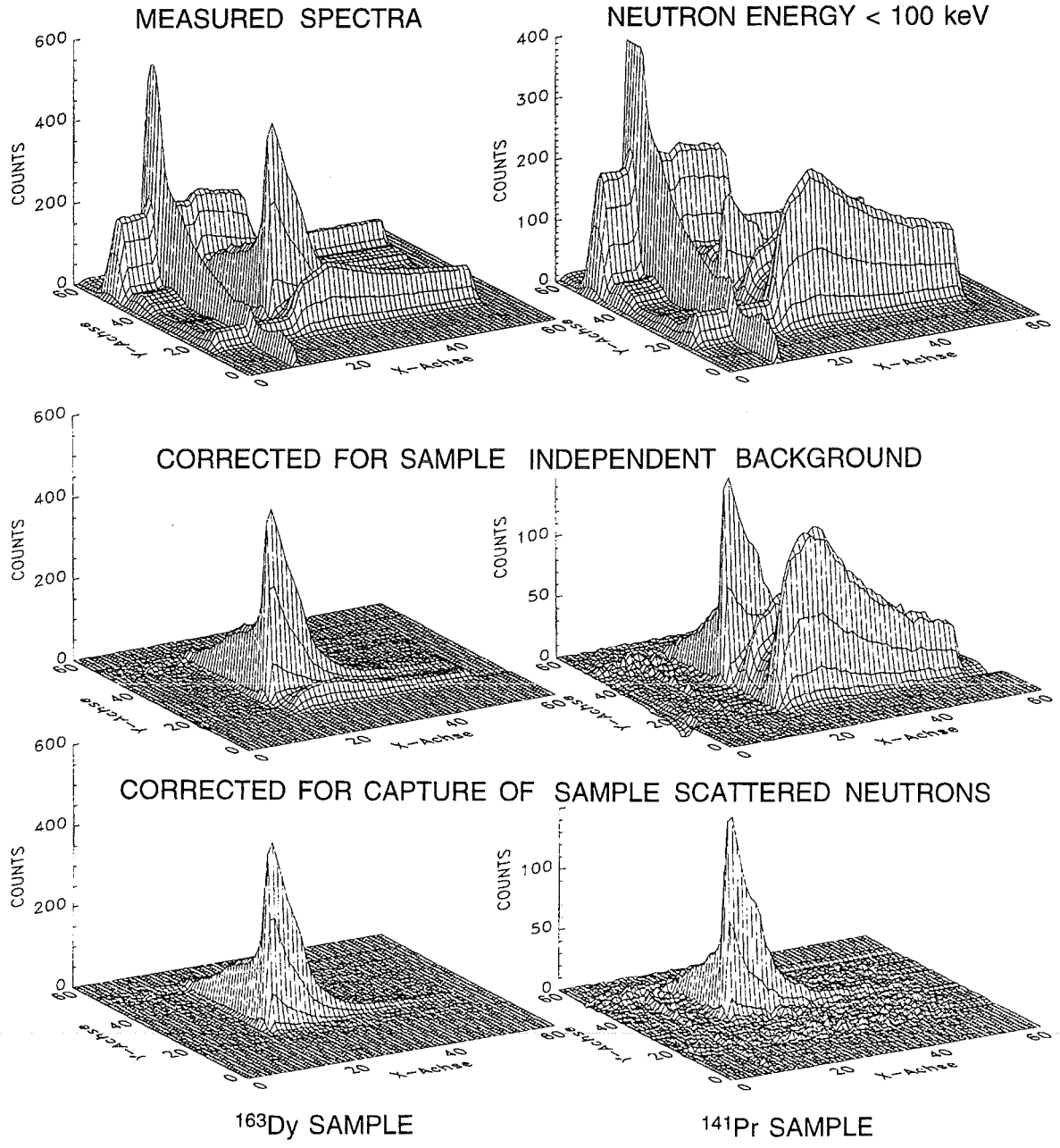

Figure 4: As Fig. 2 but for the ^{163}Dy and ^{141}Pr samples. (The small correction for isotopic impurities in the ^{163}Dy sample is omitted since it is not visible in the plot.)

For ^{160}Dy there is the peculiar situation that this sample contains more ^{161}Dy than the ^{161}Dy sample itself, resulting in a correction factor of 1.4 in the matrix (see Table 6). A sizable correction of 24% is also required to account for the ^{163}Dy impurity in the ^{164}Dy sample. For three examples the effect of the isotopic impurities is illustrated in Fig. 5, which shows the projection of the two–dimensional spectra on the sum energy axis before and after this correction. The structures due to the indicated impurities are obvious.

Table 6: MATRIX FOR ISOTOPIC CORRECTIONS (%)

Corrected spectrum	Measured spectrum					Corrected sample thickness
	^{160}Dy	^{161}Dy	^{162}Dy	^{163}Dy	^{164}Dy	(10^{-3} at/barn)
^{160}Dy	100	−140.65	−8.626	−12.240	−0.755	1.3246
^{161}Dy	−4.703	100	−1.778	−0.711	−0.083	0.7307
^{162}Dy	−0.343	−4.331	100	−12.915	−0.172	3.6202
^{163}Dy	+0.042	−0.534	−0.877	100	−2.280	1.6702
^{164}Dy	−0.317	−3.783	−1.970	−24.082	100	6.5303

In Fig. 6 the TOF spectra before subtraction of the background from isotopic impurities are shown together with this background. The correction is about 50% of the measured effect in case of the ^{160}Dy sample, but only ∼10–20% for the ^{161}Dy and ^{164}Dy samples and even less for the two other isotopes which are not shown explicitely. For the determination of the ^{160}Dy cross section the spectroscopic features of the $4\pi BaF_2$ detector become particulary important. The abundance of ^{160}Dy and ^{161}Dy in the sample is of the same order (see Table 2) but the ^{161}Dy cross section is two times larger. Accordingly, one would expect the correction to exceed the signal by the same factor. However, as can be seen from Figure 5, most of the capture events in ^{161}Dy are concentrated at energies above the ^{160}Dy peak and can be discriminated accordingly.

As discussed in Ref. [2] the present method to correct for isotopic impurities holds exactly only if all samples are about equal in weight: only then second order effects due to neutron multiple scattering and self–absorption are properly accounted for. In the present experiment the largest correction occurs for the ^{160}Dy sample due to the ^{161}Dy admixture of 37.4%. The weight of the two samples differs by a factor of 3.4. Therefore, calculating the correction directly from the isotopic matrix leads to an overcompensation due to the smaller self–shielding effect in the thin ^{161}Dy sample. With the good energy resolution of the $4\pi BaF_2$ detector, this effect can be verified in the corrected sum–energy spectrum of ^{160}Dy where a negative peak is obtained at the binding energy of ^{161}Dy. This overcompensation was removed by reducing the respective correction factor in the isotope correction matrix by 11.7%. A similar overcompensation was observed for the ^{163}Dy impurity in the ^{164}Dy sample.

Following the correction for isotopic impurities, the background due to capture of sample scattered neutrons was removed from the spectra by means of the data measured with the scattering sample. Except for ^{164}Dy and ^{141}Pr, this correction is very small due to the favorable ratios of total and capture cross sections for most isotopes. It was obtained in the same way as described in the samarium measurement [1]. After this last correction, the final spectra contain only the net capture events of the investigated isotopes (bottom spectra in Figs. 2, 3, 4, and 5). The corrections for capture of scattered neutrons are shown for all measured isotopes in Fig. 8, and the corresponding signal/background ratios are listed in Table 7 for different neutron energies.

The ^{160}Dy and ^{164}Dy spectra in the lower part of Fig. 5 exhibit small bipolar structures

at the binding energy of the respective impurity isotopes (marked by arrows). This feature, which was also observed in case of ^{144}Nd [3], is probably due to a slight shift in the position of the full energy peak in the spectra used for correction. The influence of this effect on the final cross section is negligible.

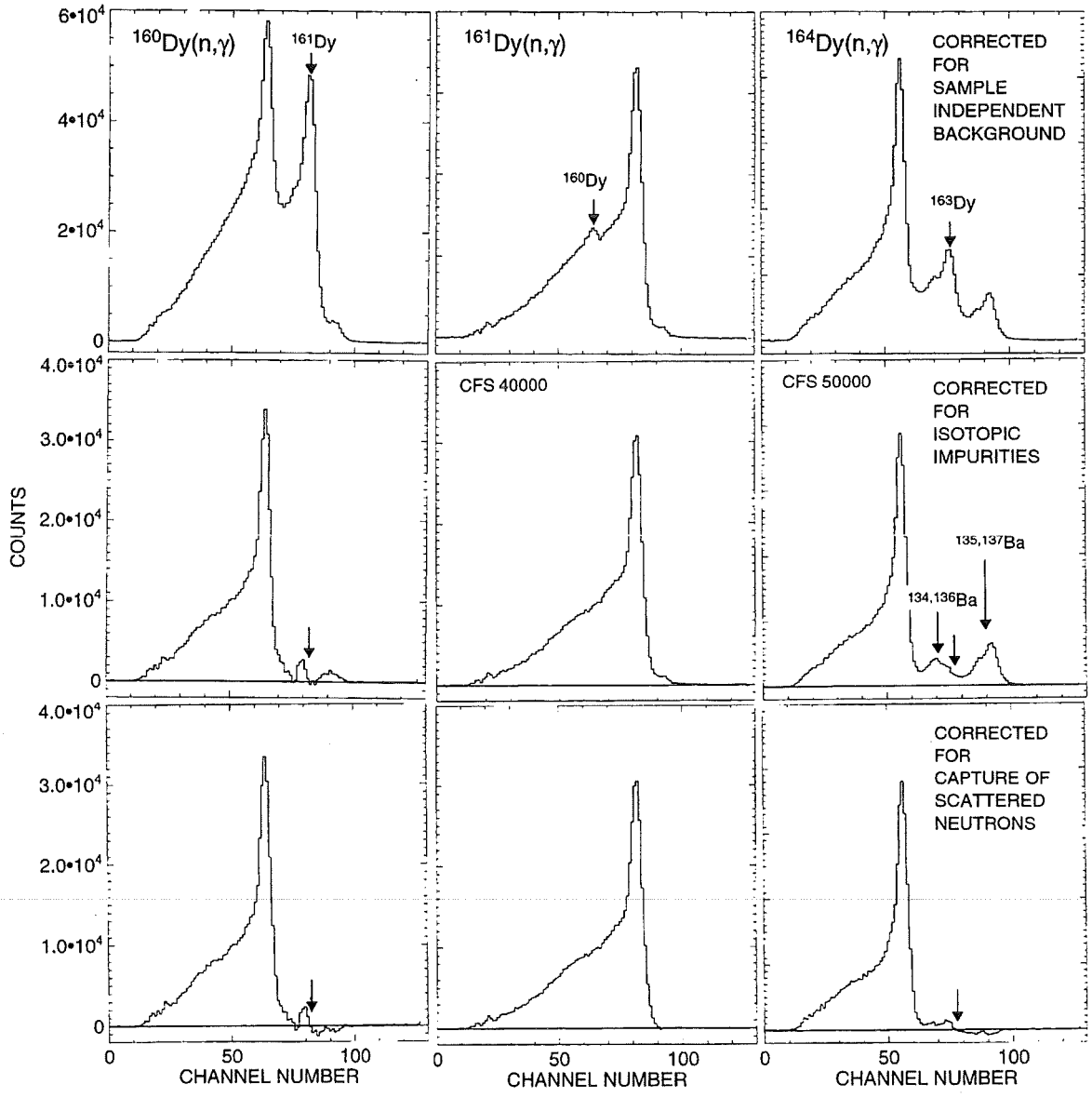

Figure 5: Sum energy spectra of the ^{160}Dy, ^{161}Dy, and ^{164}Dy samples before and after correction for isotopic impurities and capture of scattered neutrons.

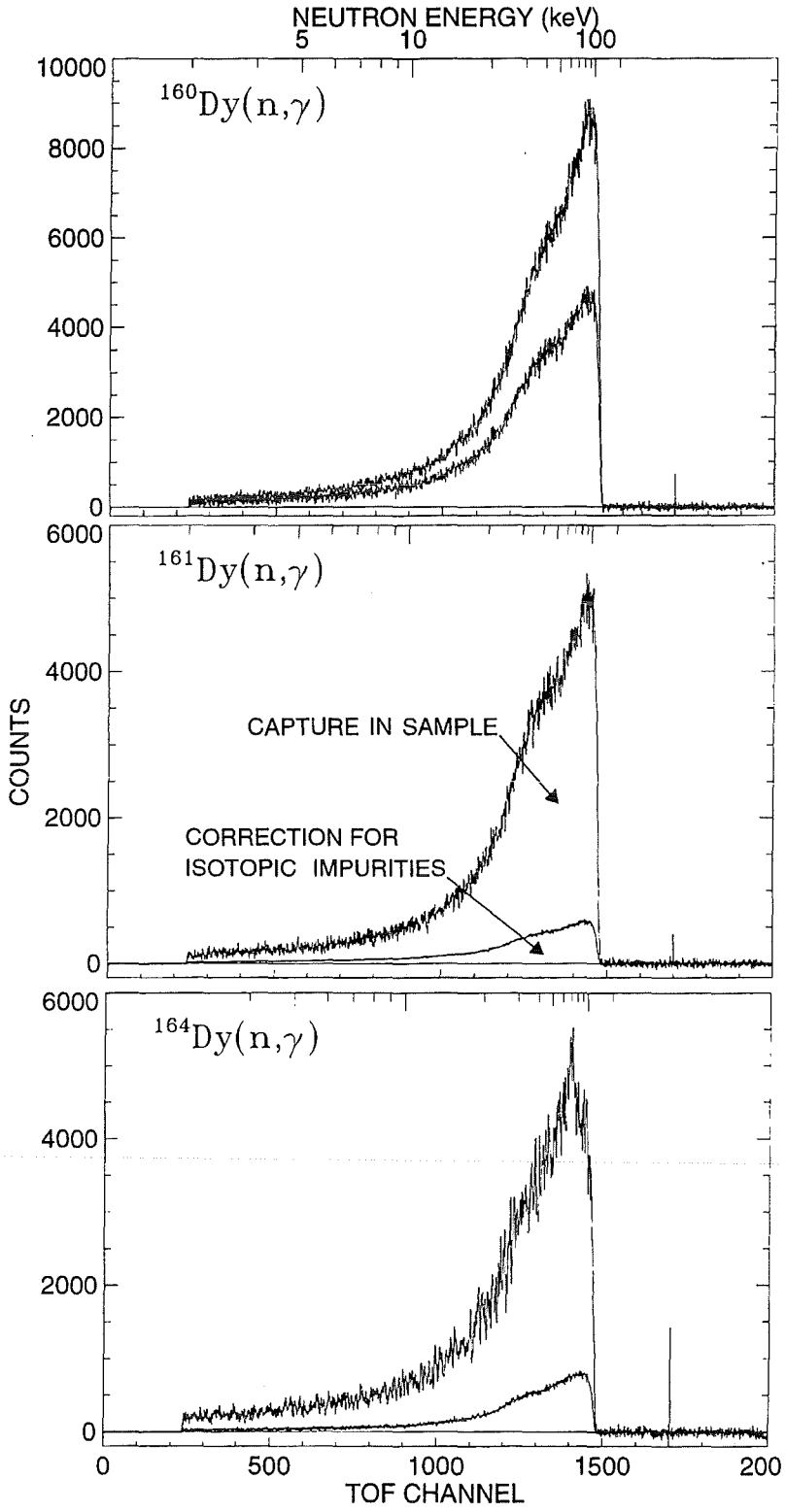

Figure 6: TOF spectra of the ^{160}Dy, ^{161}Dy, and ^{164}Dy samples. The background due to isotopic impurities is shown separately.

Table 7: SIGNAL/BACKGROUND RATIO FOR RUNS WITH DIFFERENT MAXIMUM NEUTRON ENERGY

Sample	σ_t/σ_γ[a]	Maximum neutron energy	Signal/Background ratio[b]		
	E_n=30 keV	(keV)	E_n=30 keV	E_n=20 keV	E_n=10 keV
^{160}Dy	18	100	11.3	5.5	3.5
^{161}Dy	8.5		11.9	5.6	3.0
^{162}Dy	35		7.8	3.9	2.3
^{163}Dy	13		8.6	4.3	2.7
^{164}Dy	74		5.4	3.1	1.8
^{141}Pr	129		3.2	1.9	1.5
^{197}Au	24		11.2	5.0	3.5
^{160}Dy		200	8.4	4.6	2.8
^{161}Dy			9.5	5.5	2.8
^{162}Dy			5.6	3.1	1.7
^{163}Dy			6.9	3.9	2.3
^{164}Dy			3.9	2.3	1.6
^{141}Pr			2.4	1.8	1.3
^{197}Au			8.0	4.1	2.8

[a]Total cross section including oxygen

[b]Defined as (effect+neutron scattering background)/(neutron scattering background)

In the first run of the present experiment two scattering samples, ^{208}Pb and graphite, were mounted on the sample ladder to check for possible systematic differences. The ratio of both evaluations is plotted in Fig. 7 for ^{164}Dy and ^{160}Dy which give rise to large and small scattering corrections, respectively. The mean values of these ratios are 1.003 and 0.999, similar to all other isotopes. Hence, any systematic uncertainties due to the mass difference of the investigated isotopes and the nuclei used for the scattering correction can be excluded.

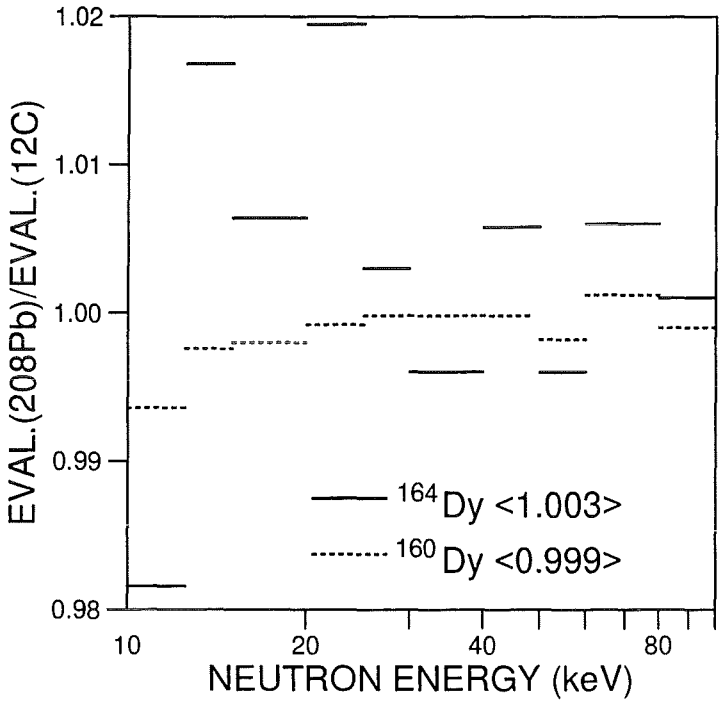

Figure 7: Ratio of the neutron capture cross sections measured with the ^{208}Pb and the graphite sample for simulating the background from scattered neutrons.

After subtraction of the scattering background the cross section shape versus neutron energy was determined from the TOF spectra of Fig. 8. For normalization, the two-dimensional data were projected onto the sum energy axis using the TOF region with optimum signal/background ratio as indicated in Fig. 8 by dashed boxes. The resulting pulse height spectra are shown in Fig. 9 for the events with multiplicity >2. The threshold in sum energy is 1.6 MeV.

The sum energy spectra of all isotopes are shown in Fig. 10 for different multiplicities. These multiplicities correspond to the number of detector modules contributing per event, which are slightly smaller than the true multiplicities because of cross talking. In the even dysprosium isotopes, 25 to 40% of the capture events are observed with multiplicities $\geq$5, while the respective fraction in the odd isotopes is about 50–60%. In contrast, the neutron magic, odd isotope ^{141}Pr exhibits a comparably low multiplicity. The arrows in Fig. 10 indicate the range of sum energy channels that were integrated to obtain the TOF spectra of Fig. 8 for determining the cross section shapes.

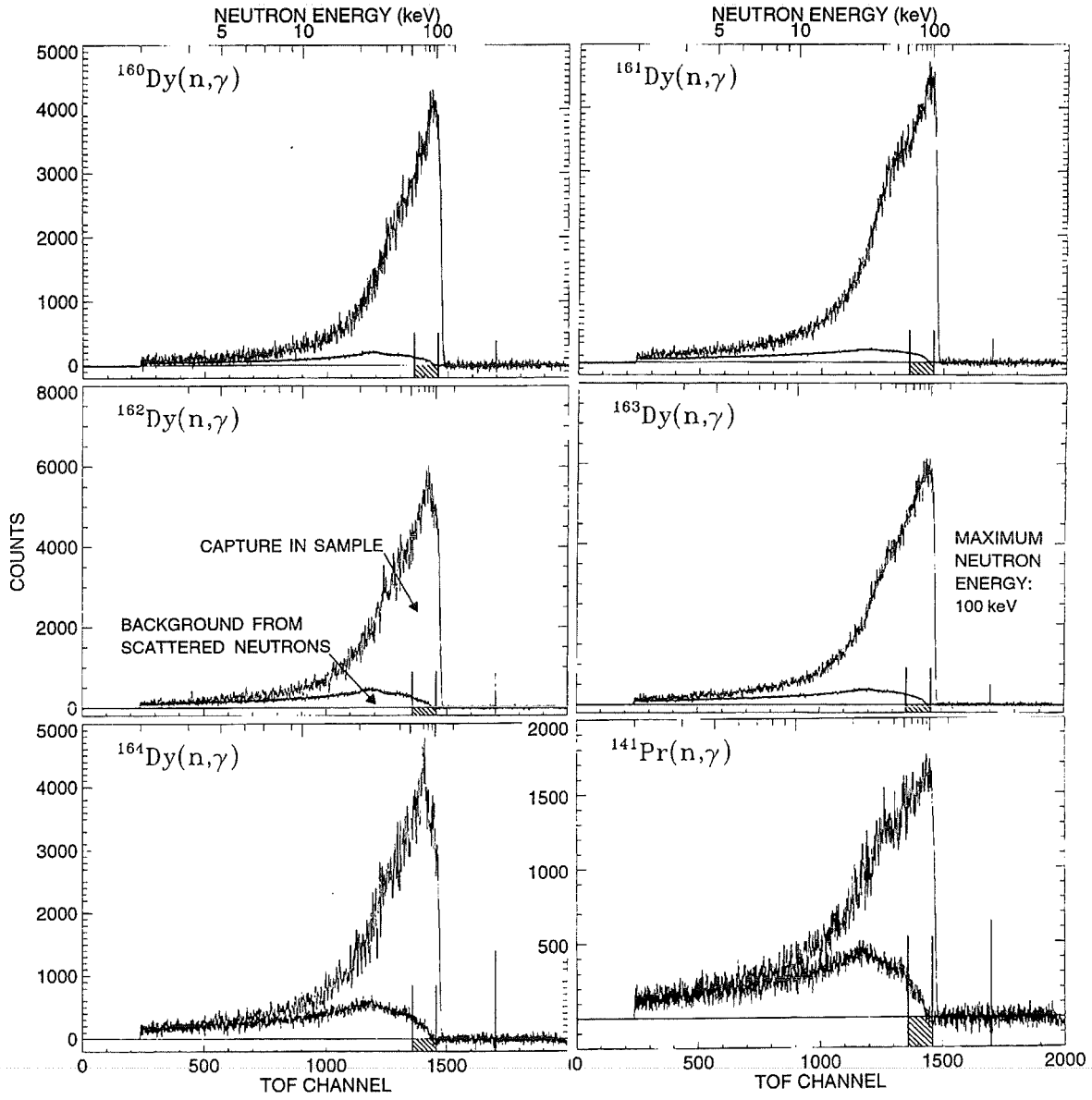

Figure 8: TOF spectra measured with the neodymium samples in Run III (100 keV maximum neutron energy). The background due to sample scattered neutrons is shown separately. The region used for absolute normalization of the cross section is indicated by hatched boxes.

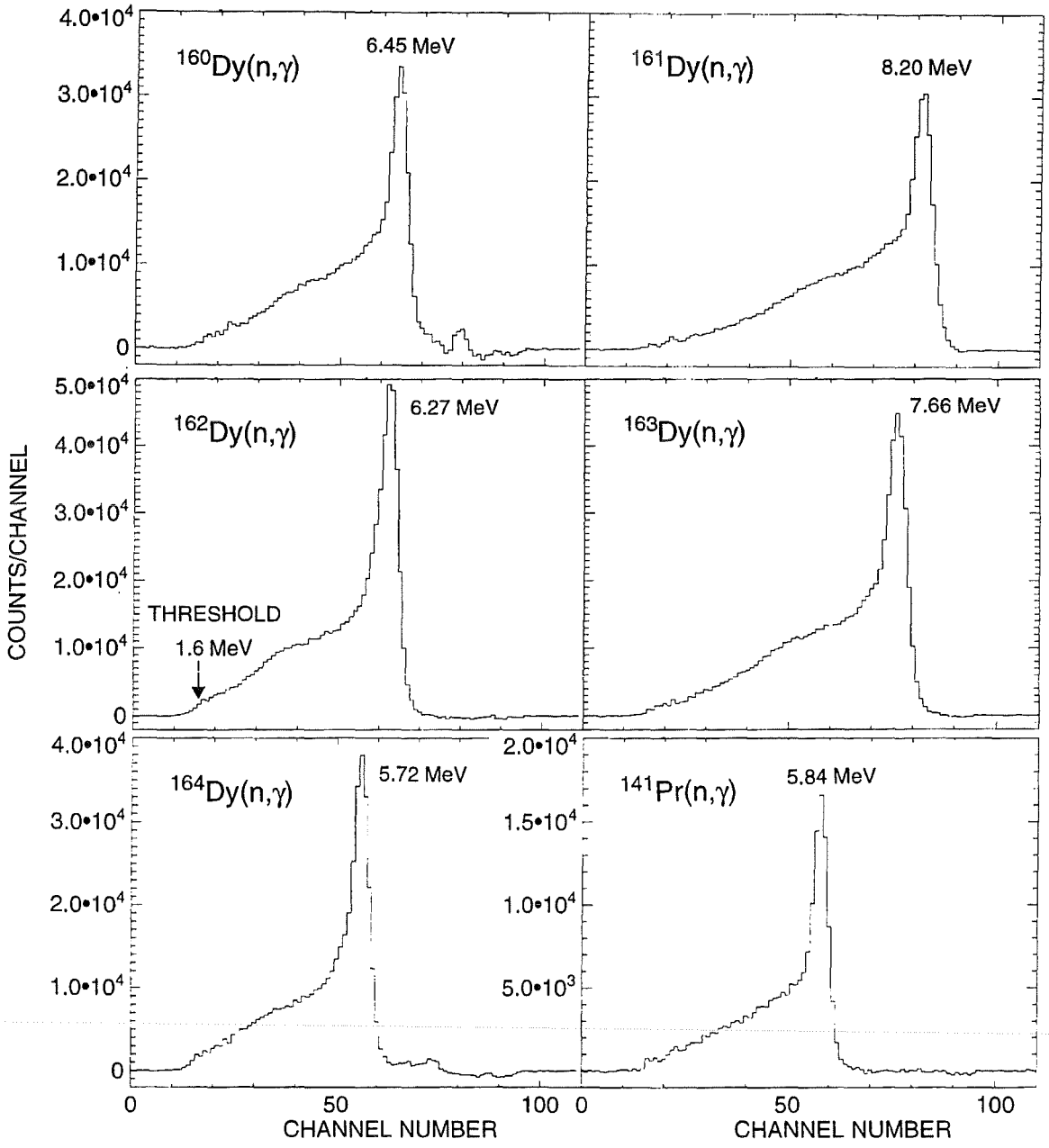

Figure 9: Sum energy spectra of all isotopes measured in Run III containing events with multiplicity >2. These spectra were obtained by projection of the two-dimensional spectra in the TOF region below the maximum neutron energy as indicated by hatched boxes in Fig. 8.

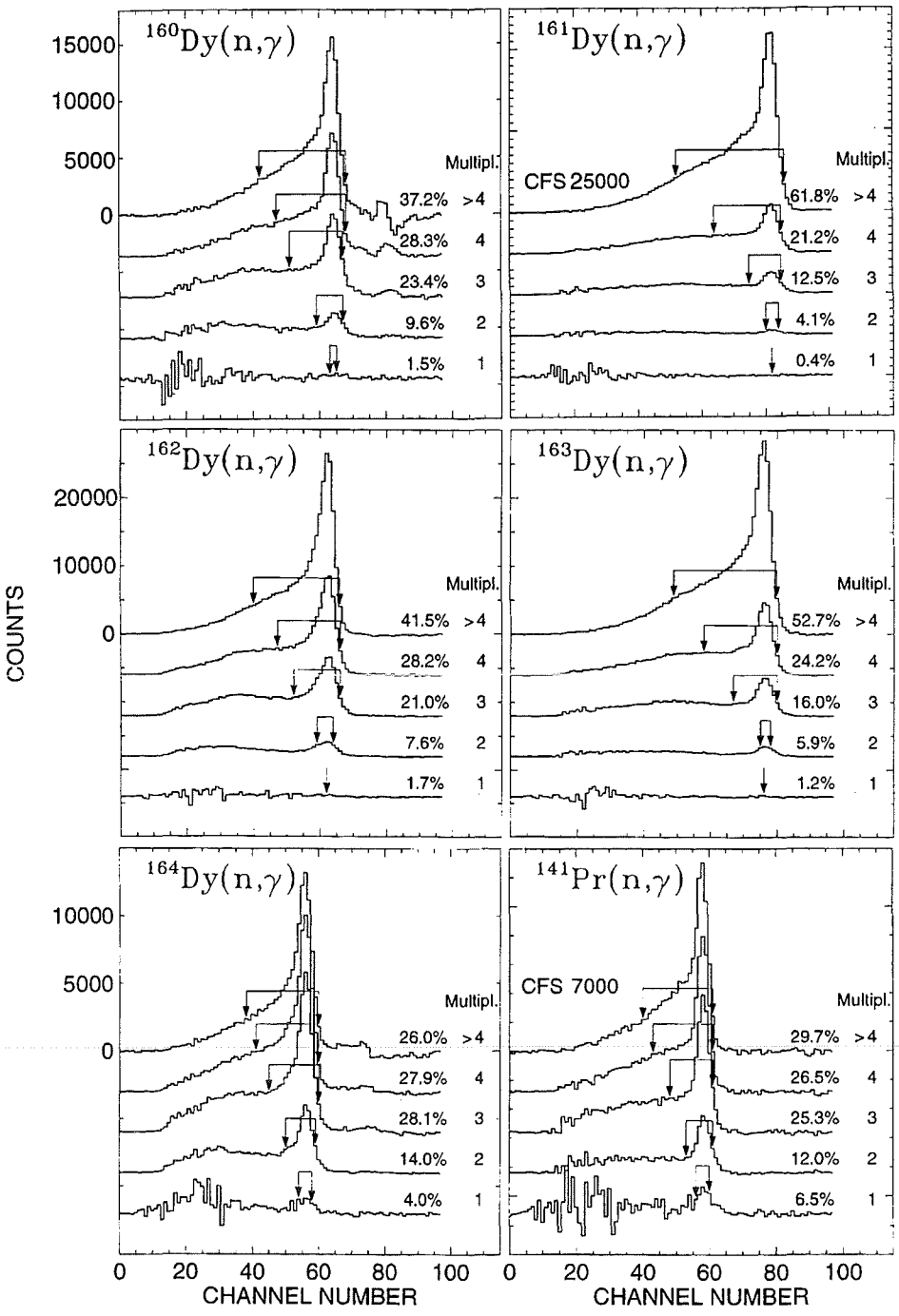

Figure 10: Sum energy spectra of all isotopes as a function of multiplicity. The regions used to determine the cross section shape are indicated by arrows.

The cross section ratio of isotope X relative to the gold standard is given by

$$\frac{\sigma_i(X)}{\sigma_i(Au)} = \frac{Z_i(X)}{Z_i(Au)} \cdot \frac{\Sigma Z(Au)}{\Sigma Z(X)} \cdot \frac{\Sigma E(X)}{\Sigma E(Au)} \cdot \frac{m(Au)}{m(X)} \cdot F_1 \cdot F_2. \quad (1)$$

In this expression, Z_i is the count rate of channel i in the TOF spectrum, ΣZ is the TOF rate integrated over the interval used for normalization (Fig. 8), ΣE is the total count rate in the sum energy spectrum for all multiplicities summed over the normalization interval (Fig. 10), and m is the sample thickness in atoms/barn. The factor F_1 = (100–f(Au))/(100–f(X)) corrects for the fraction of capture events f below the experimental threshold in sum energy, where X refers to the respective dysprosium sample (Table 8), and F_2 is the ratio of the multiple scattering and self–shielding corrections.

The fraction of unobserved capture events, f, and the correction factor F_1 were calculated as described in Ref. [14]. The input for this calculation are the individual neutron capture cascades and their relative contributions to the total capture cross section as well as the detector efficiency for monoenergetic γ–rays in the energy range up to 10 MeV. In contrast to previous experiments, where the capture cascades have been calculated via the statistical and optical model [23, 24], this information was derived directly from the experimental data recorded with the ADC system in Run III. From these data, only events close to the sum energy peak (see Fig. 9) were selected, which contained the full capture γ–ray cascade. This ensemble was further reduced by restricting the analysis to the TOF region with optimum signal to background ratio (dashed areas in Fig. 8).

The energy of the individual γ–rays in the cascade were then normalized such that the sum energy corresponds exactly to the respective binding energy. In this way about 100000 cascades were derived for each sample to replace the theoretical cascades in the calculation of the sum–energy spectra. The calculation was performed in the same way as described previously [3], using the response functions of the $4\pi BaF_2$ detector for monoenergetic γ–rays. In view of the large number of cascades, Monte Carlo methods had to be used in these calculations. This fast approach has been shown to provide a very good approximation compared to the exact solution [3].

The remaining background in the calculated sum energy spectra was corrected by subtracting the contributions from cascades measured with the dummy sample and the carbon sample. These were extracted in the same sum energy and TOF intervals as used for the measured isotope. For the example of ^{155}Gd, the various background components are compared with the true spectrum in Fig. 11.

The capture cascades determined in this way are still disturbed by cross–talk effects, but the high density and the relatively large volume of the BaF_2 crystals requires only a comparably small correction. While the number of modules which contributed per event yields an upper limit for the multiplicity, a corresponding lower limit was obtained by assuming that hits in neighboring crystals were always due to a single γ–ray. Since there is a $\sim$15% probability that two γ–rays of the same cascade hit neighboring crystals, the true multiplicity should lie somewhere between these two extremes. In addition the two evaluation methods with and without rejecting background from scattered neutrons, were applied as well. Hence, four sets of correction factors F_1 were calculated for each sample, the average yielding the adopted values quoted in Table 8.

The reliability of the new determination of the correction factors F_1 was checked by repeating the evaluation for the respective values of the gadolinium isotopes [2] which had been obtained from two independent theoretical calculations by G. Reffo and M. Uhl. The upper part of Fig. 12 shows the individual results of the four evaluations compared to the adopted corrections of Ref. [2]. The individual results for the even and odd isotopes agree to better than $\pm 0.15\%$ and $\pm 0.4\%$, respectively, but their mean is lower by $\sim 0.5\%$ than the theoretical corrections. From the lower part of Fig. 12, where only the mean values are given, obviously perfect agreement is obtained within the quoted uncertainties of Ref. [2] if the new values are normalized by a factor of 1.005. This agreement shows that the difference is mainly due to problems in determining the capture cascades for the gold standard. The correlated uncertainty of $\pm 0.25\%$ is, however, small compared to the overall uncertainty of 1.5% that has to be considered for the capture cross section of gold. Moreover, it cancels out in most astrophysical applications, where only the relative uncertainties of the individual gadolinium isotopes are important. In summary, the determination of the correction factor F_1 from experimental data was shown to be a reliable alternative which can be used for the present investigation as well as in future work.

The capture γ-ray spectra deduced from the data taken with the ADC system are shown in Fig. 13 in energy bins of 500 keV. It is interesting to note significant structures between 2 and 3 MeV in all Dy isotopes as well as the hard components in the ^{141}Pr and ^{164}Dy spectra, the two isotopes with the lowest cascade multiplicities.

The final sum energy spectra calculated from the measured capture cascades in Fig. 14 show good agreement compared to the experimental spectra of Fig. 9. Due to the low γ–threshold of 1.5 - 1.8 MeV the detection efficiency for the capture cascades of the investigated dysprosium isotopes exceeds 96% despite of their comparably low binding energies down to 5.7 MeV. As in all previous experiments with the 4π BaF_2 detector, the correction factor F_1 was found to depend linearly on the binding energy of the captured neutron.

The correction for neutron multiple scattering and self–shielding was calculated with the SESH code [17]. Apart from the pairing energies [25], most of the input parameters were taken from Ref. [26] but were slightly modified in order to reproduce the measured total and capture cross sections. The final values are listed in Table 9 together with the calculated total cross sections. The resulting correction factors, MS(X) and F_2, are compiled in Tables 10 and 11.

Since the enrichment of some samples is comparably low, these corrections were calculated either for the true sample composition or for that part which remains after the correction for isotopic impurities. It was assumed, that subtraction of the isotopic impurities via the normalized spectra of the other samples accounts for the respective contributions to the multiple scattering corrections as well. Therefore, the cross section was determined using the corrections calculated as if the samples consisted of the main isotopes only. In general, these corrections are below 2% except for the even isotopes at energies below 10 keV.

Table 8: FRACTION OF UNDETECTED CAPTURE EVENTS, f (%), AND THE RELATED CORRECTION FACTORS F_1. [a]

	Threshold in Sum Energy (MeV)			
	1.5	1.6	1.8	2.0
f(Au)	4.62			6.54
f(^{152}Gd)	2.19			3.50
f(^{154}Gd)	2.01			3.26
f(^{155}Gd)	0.60			1.08
f(^{156}Gd)	2.27			3.64
f(^{157}Gd)	1.07			1.76
f(^{158}Gd)	2.94			4.53
F_1(^{152}Gd/Au)	0.975			0.969
F_1(^{154}Gd/Au)	0.973			0.966
F_1(^{155}Gd/Au)	0.960			0.945
F_1(^{156}Gd/Au)	0.976			0.970
F_1(^{157}Gd/Au)	0.964			0.951
F_1(^{158}Gd/Au)	0.983			0.979
f(Au)	4.85			6.76
f(^{160}Dy)	2.27			3.53
f(^{161}Dy)	0.94			1.59
f(^{162}Dy)	2.83			4.18
f(^{163}Dy)	1.40			2.27
f(^{164}Dy)	3.54			5.37
f(^{141}Pr)	3.79			5.71
F_1(^{160}Dy/Au)	0.974	0.972	0.969	0.966
F_1(^{161}Dy/Au)	0.960	0.957	0.952	0.947
F_1(^{162}Dy/Au)	0.979	0.978	0.975	0.973
F_1(^{163}Dy/Au)	0.965	0.963	0.958	0.954
F_1(^{164}Dy/Au)	0.986	0.986	0.985	0.985
F_1(^{141}Pr/Au)	0.989	0.989	0.989	0.989

[a] derived from capture cascades measured with the ADC system.

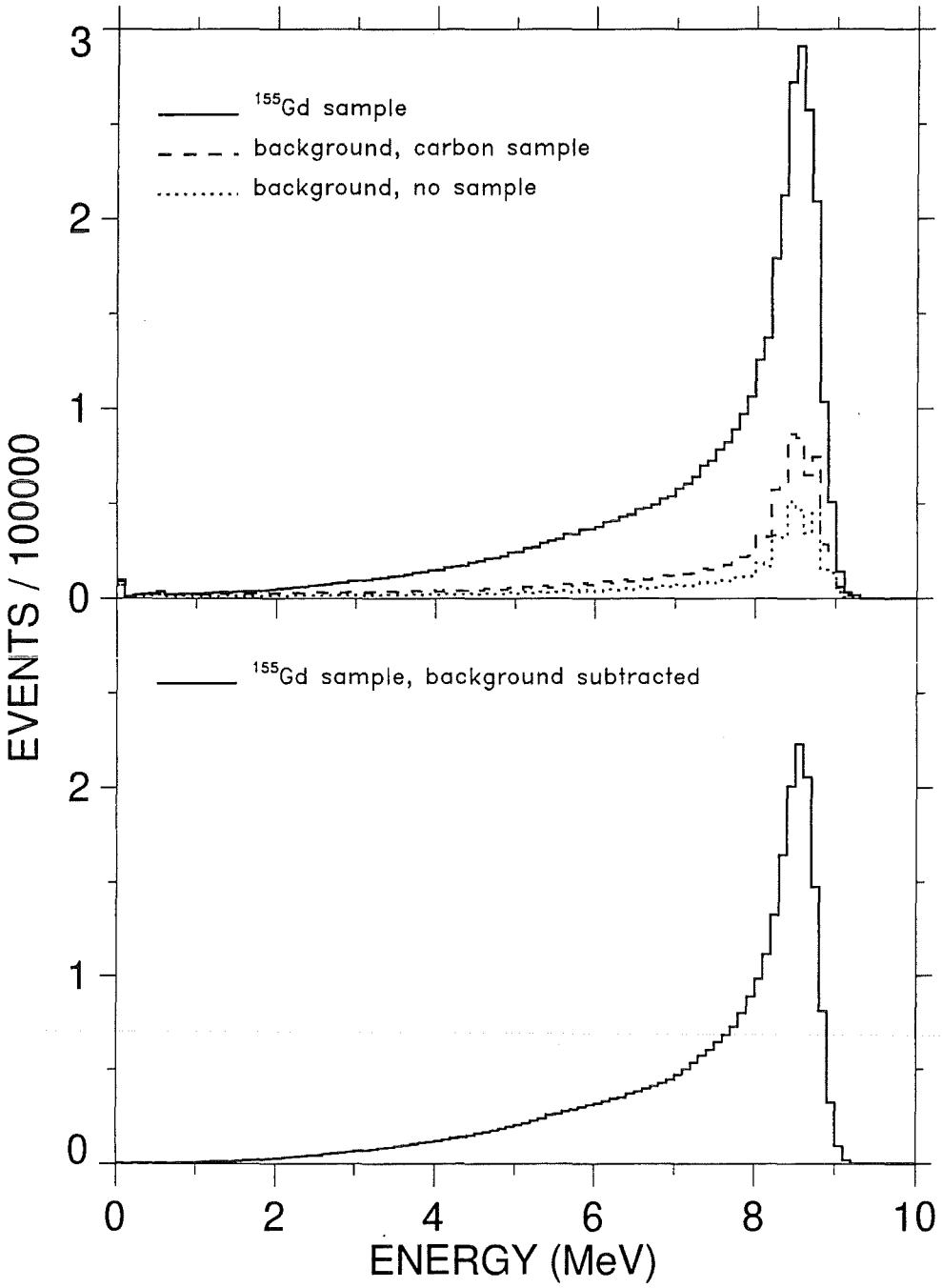

Figure 11: Sum energy spectra from sample, carbon sample and empty canning as calculated from experimental capture cascades (top) and the corrected spectrum for the example of neutron captures on ^{155}Gd (bottom).

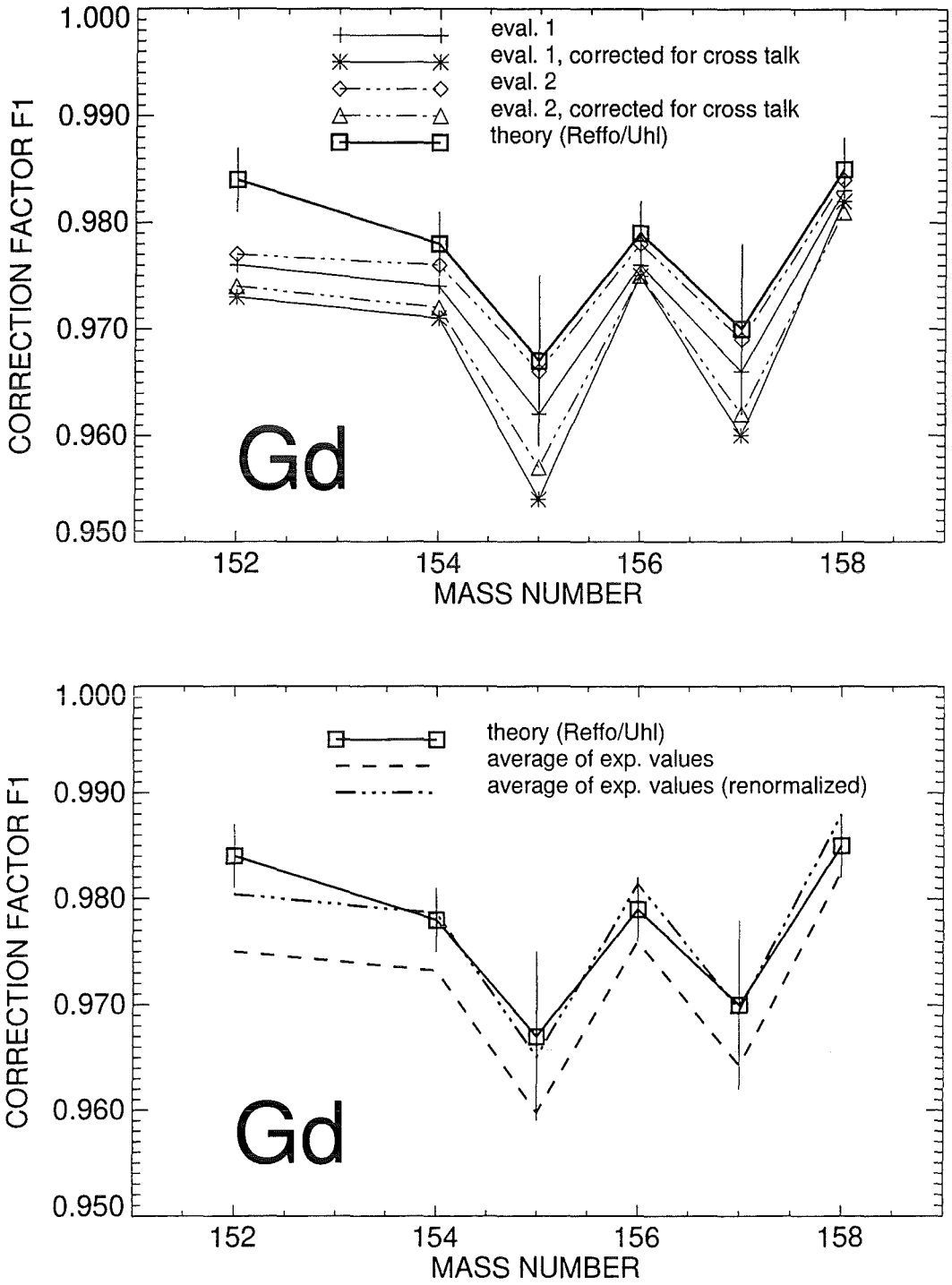

Figure 12: The correction factor F_1 for the gadolinium isotopes evaluated from experimental capture cascades compared to the data of Ref. [2] which were derived from theoretical capture cascades. The upper part shows the results of the four individual calculations. Perfect agreement is found if the new values are normalized by a factor of 1.005 (lower part).

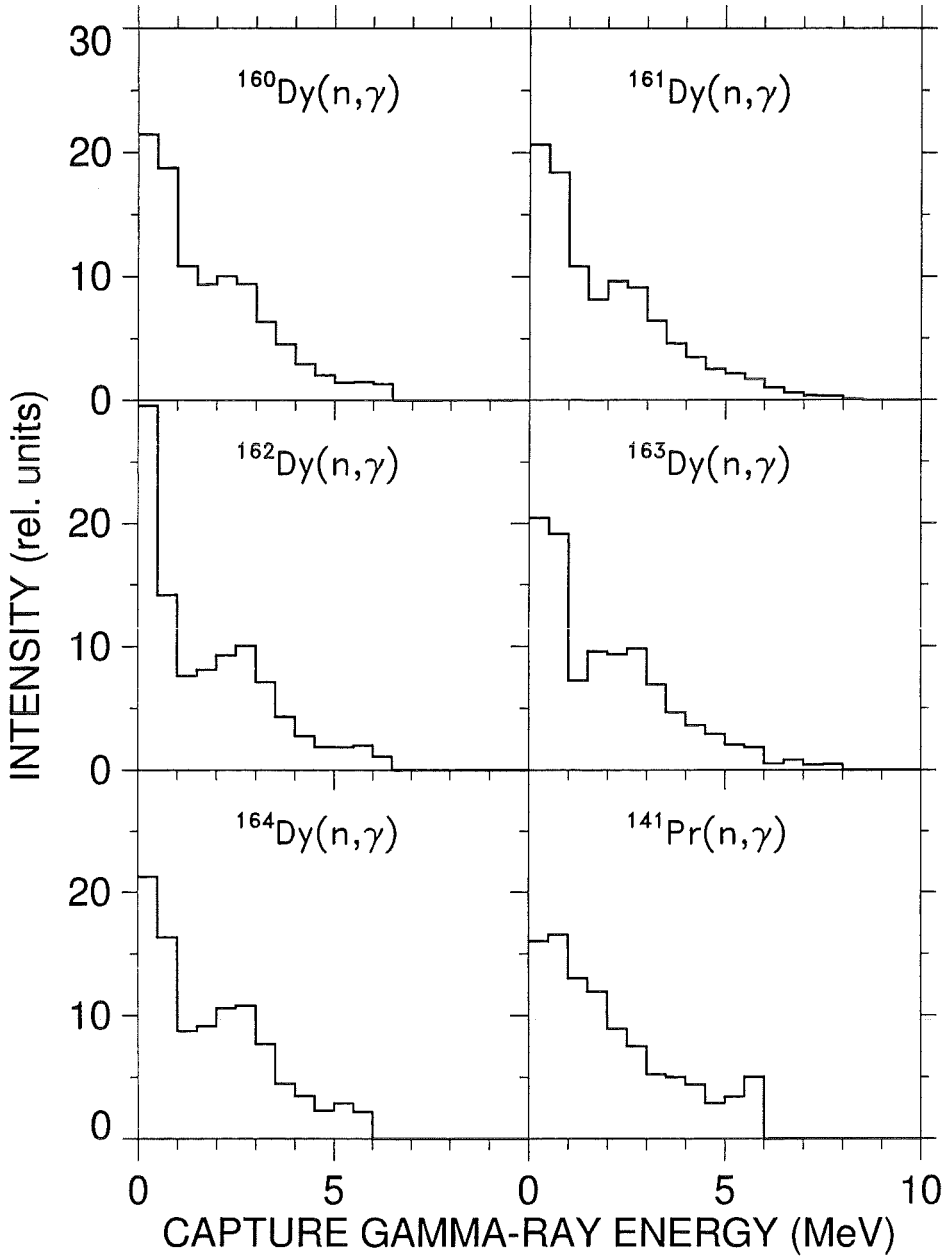

Figure 13: Capture γ–ray spectra derived from the capture cascades recorded with the ADC system.

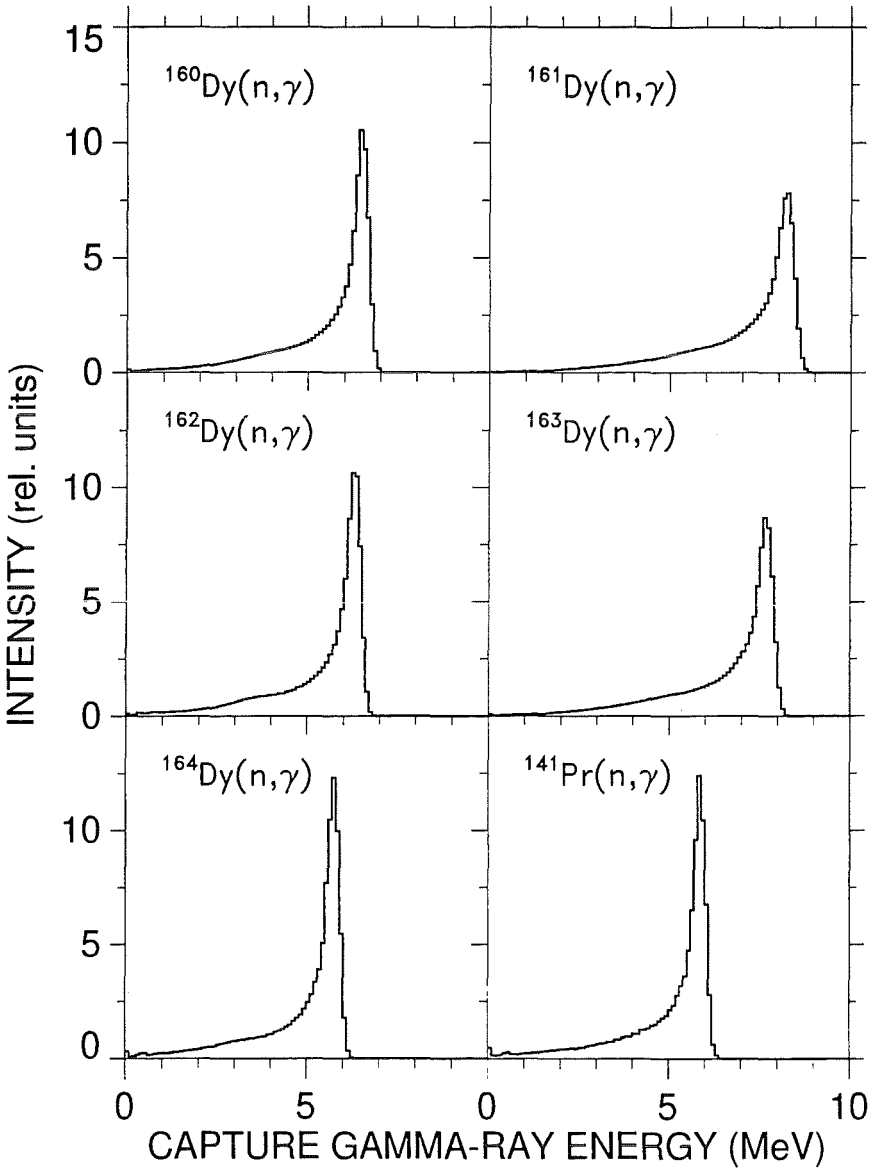

Figure 14: Calculated sum energy spectra of the $4\pi BaF_2$ detector based on experimental capture cascades and measured lineshapes. These spectra were used to derive the correction F_1 for unobserved capture events.

Table 9: PARAMETERS FOR THE CALCULATION OF NEUTRON SELF-SHIELDING AND MULTIPLE SCATTERING CORRECTIONS

Parameter		^{160}Dy	^{161}Dy	^{162}Dy	^{163}Dy	^{164}Dy	^{141}Pr	^{16}O
Nucleon Number		160	161	162	163	164	141	16
Binding Energy (MeV)		6.454	8.197	6.271	7.658	5.716	5.844	4.144
Pairing Energy (MeV)		0.92	1.62	0.92	1.79	0.92	0.0	0.0
Effective Temperature (K)		293	293	293	293	293	293	293
Nuclear Spin		0	2.5	0	2.5	0	2.5	0
Average Radiation	s	0.146	0.152	0.100	0.146	0.120	0.090	0.0
Width (eV)	p	0.044	0.022	0.060	0.060	0.040	0.050	0.0
	d	0.002	0.002	0.002	0.002	0.002	–	0.0
Average Level	s	27.	2.67	64.6	6.85	147.	88.	0.0
Spacing (eV)	p[a]	9.	1.34	21.5	3.43	49.0	44.	0.0
	d[a]	5.4	0.89	12.9	2.28	29.4	–	0.0
Strength Function	S_0	1.6	2.0	1.5	1.9	1.4	1.5	0.0
(10^{-4})	S_1	1.5	1.5	1.5	1.0	1.5	0.3	0.0
	S_2	2.0	1.0	0.7	0.7	0.7	–	0.0
Nuclear Radius	s	7.2	8.0	7.8	7.5	7.5	4.9	5.5
(fm)	p	7.2	8.0	7.8	7.5	7.5	4.9	0.0
	d	7.2	8.0	7.8	7.5	7.5	–	0.0
		Calculated total cross sections						
3 keV		18.7	23.1	19.0	21.4	17.7	14.4	3.80
5 keV		16.0	19.7	16.5	18.1	15.4	11.8	3.80
10 keV		13.3	16.2	13.9	14.8	13.0	9.19	3.79
20 keV		11.3	13.7	12.1	12.4	11.3	7.33	3.77
40 keV		9.93	11.8	10.7	10.6	10.1	7.24	3.74
80 keV		8.89	10.3	9.61	9.14	9.10	5.04	3.68
160 keV		8.05	8.93	8.59	7.90	8.24	4.37	3.55
320 keV		7.37	7.60	7.56	6.80	7.38	4.00	3.31

[a]Calculated with SESH [17]

Table 10: CORRECTION FACTORS FOR NEUTRON SELF-SHIELDING AND MULTIPLE SCATTERING, MS

Energy Bin	MS						
(keV)	^{197}Au	^{160}Dy	^{161}Dy	^{162}Dy	^{163}Dy	^{164}Dy	^{141}Pr
3 – 5	0.997	0.974	1.007	0.902	1.005	0.788	0.864
5 – 7.5	1.017	0.991	1.009	0.955	1.013	0.869	0.927
7.5 – 10	1.026	0.998	1.010	0.982	1.018	0.914	0.959
10 – 12.5	1.030	1.002	1.011	0.997	1.020	0.936	0.975
12.5 –15	1.033	1.003	1.011	1.004	1.021	0.952	0.984

Table 10 (continued)

15 – 20	1.035	1.005	1.012	1.011	1.021	0.968	0.994
20 – 25	1.036	1.007	1.012	1.016	1.021	0.980	1.002
25 – 30	1.036	1.007	1.012	1.018	1.021	0.988	1.007
30 – 40	1.036	1.008	1.011	1.020	1.022	0.995	1.012
40 – 50	1.035	1.009	1.011	1.021	1.022	1.000	1.016
50 – 60	1.034	1.009	1.011	1.021	1.021	1.004	1.018
60 – 80	1.033	1.010	1.011	1.022	1.020	1.009	1.020
80 – 100	1.032	1.010	1.011	1.022	1.020	1.012	1.021
100 – 120	1.030	1.009	1.010	1.022	1.020	1.013	1.021
120 – 150	1.029	1.009	1.010	1.022	1.019	1.014	1.021
150 – 175	1.028	1.008	1.010	1.022	1.019	1.016	1.021
175 – 200	1.027	1.008	1.010	1.022	1.019	1.017	1.021
200 – 225	1.026	1.008	1.009	1.022	1.018	1.018	1.021
Uncertainty (%)	0.3	0.6	0.2	0.3	0.2	0.5	0.3

Table 11: CORRECTION FACTORS FOR THE CROSS SECTION RATIOS, F_2 = MS(Au)/MS(X)

Energy Bin	F_2					
(keV)	^{160}Dy/Au	^{161}Dy/Au	^{162}Dy/Au	^{163}Dy/Au	^{164}Dy/Au	^{141}Pr/Au
3 – 5	1.022	0.988	1.103	0.990	1.263	1.152
5 – 7.5	1.025	1.007	1.064	1.003	1.169	1.096
7.5– 10	1.029	1.017	1.046	1.009	1.124	1.071
10 – 12.5	1.030	1.021	1.035	1.012	1.103	1.058
12.5 – 15	1.032	1.024	1.031	1.014	1.087	1.052
15 – 20	1.032	1.025	1.026	1.016	1.071	1.043
20 – 25	1.030	1.025	1.021	1.016	1.058	1.035
25 – 30	1.029	1.024	1.018	1.015	1.049	1.029
30 – 40	1.028	1.025	1.016	1.014	1.041	1.024
40 – 50	1.026	1.024	1.014	1.013	1.035	1.019
50 – 60	1.025	1.023	1.013	1.013	1.030	1.016
60 – 80	1.023	1.022	1.011	1.013	1.024	1.013
80 – 100	1.022	1.021	1.010	1.012	1.020	1.011
100 – 120	1.021	1.020	1.008	1.010	1.017	1.009
120 – 150	1.020	1.019	1.007	1.010	1.015	1.008
150 – 175	1.020	1.018	1.006	1.009	1.012	1.007
175 – 200	1.019	1.017	1.005	1.008	1.010	1.006
200 – 225	1.018	1.017	1.004	1.008	1.008	1.005
Uncertainty (%)	0.7	0.4	0.4	0.4	0.6	0.4

4 RESULTS FOR THE NEUTRON CAPTURE CROSS SECTIONS

The measured neutron capture cross section ratios of the investigated Dy isotopes, and of ^{197}Au are listed in Tables 12 to 17 together with the respective statistical uncertainties. The data are given for all runs and for the two evaluation methods discussed in Sec. 3. The last column in each table contains the weighted average, the weight being determined by the inverse of the squared statistical uncertainties. Since the cross section ratios depend weakly on energy, the averages for the energy interval from 30 to 80 keV are also included for a better comparison of the individual results. The data are free of systematic differences with respect to different runs or evaluations. This is important as they were obtained with different data acquisition modes, scattering samples, and neutron spectra. For example the results from Evaluation 1 – for the average of all samples – exceed those of Evaluation 2 by only 0.8%, a difference which is just opposite as for the neodymium isotopes [3]. The largest discrepancy is found for the results of the two evaluations for ^{161}Dy and ^{163}Dy which differ by 2%. All these differences, however, are well compatible with the respective statistical uncertainties.

As in the previous measurements with the 4π BaF_2 detector [1, 12, 27], the final cross section ratios were adopted from Evaluation 2. The respective mean values are compiled for all runs in Table 18 together with the statistical, systematic, and total uncertainties. The energy bins are sufficiently fine to avoid systematic uncertainties in the calculation of the Maxwellian averaged cross sections (Sec. 6). The final uncertainties of the cross section ratios are less than 1.4% for all isotopes in the energy range from 30 to 100 keV but reach 12% at the lowest energy bin in case of ^{141}Pr.

The experimental ratios were converted into absolute cross sections using the gold cross section of Macklin [28] after normalization by a factor of 0.989 to the absolute value of Ratynski and Käppeler [29] (Table 19). The uncertainties of these data can be obtained by adding the 1.5% uncertainty of the reference cross section to the uncertainties of the respective cross section ratios.

The present results are compared to previous data in Figs. 15 to 17. For all five dysprosium isotopes very good agreement is found with the results of Kononov *et al.* [30] which are quoted with uncertainties of 5 – 10%. There is also good agreement with the results of Beer *et al.* for ^{161}Dy and ^{163}Dy [31, 32], but the important *s*–only isotope ^{160}Dy shows a severe discrepancy. The data of Igashira, which are given without uncertainty [33], are significantly different from the present results for all three dysprosium isotopes. In case of ^{141}Pr good agreement is found with the data of Taylor *et al.* [34] and Gibbons *et al.* [35]. Again, the data of Igashira [33] show a significant deviation. In all cases, the uncertainties of the present data are much smaller than in all previous measurements.

Table 12: $\sigma(^{160}\mathrm{Dy})/\sigma(^{197}\mathrm{Au})$ AND STATISTICAL UNCERTAINTIES IN (%)

Energy Bin (keV)	Run I		Run II		Run III		Average	
Evaluation 1								
3 – 5	1.5138	4.7	0.8944	18.	1.0005	9.3	1.3806	4.2
5 – 7.5	1.2548	2.9	1.2250	7.6	1.0595	5.7	1.2151	2.5
7.5 – 10	1.4791	2.5	1.3259	5.5	1.4927	3.8	1.4634	2.0
10 – 12.5	1.3167	2.1	1.1980	4.7	1.2447	3.2	1.2839	1.6
12.5 – 15	1.4930	1.7	1.4297	3.8	1.4959	2.6	1.4860	1.3
15 – 20	1.4788	1.1	1.4632	2.3	1.4678	1.6	1.4738	0.9
20 – 25	1.6331	1.0	1.5700	1.9	1.6497	1.4	1.6281	0.7
25 – 30	1.5983	0.9	1.5913	1.6	1.6049	1.2	1.5989	0.6
30 – 40	1.6741	0.6	1.6620	1.1	1.6550	0.9	1.6668	0.5
40 – 50	1.8045	0.6	1.7522	1.1	1.7867	0.9	1.7906	0.5
50 – 60	1.7211	0.6	1.7587	1.1	1.7489	0.9	1.7342	0.5
60 – 80	1.7215	0.5	1.7390	0.9	1.7517	0.8	1.7322	0.4
80 – 100	1.7323	0.5	1.7014	0.9	1.7517	0.8	1.7317	0.4
100 – 120	1.5009	0.6	1.5048	1.0	1.5493	0.9	1.5140	0.5
120 – 150	–	–	1.4221	0.9	–	–	1.4221	0.9
150 – 175	–	–	1.3269	1.0	–	–	1.3269	1.0
175 – 200	–	–	1.2484	1.1	–	–	1.2484	1.1
200 – 225	–	–	1.1975	1.8	–	–	1.1975	1.8
30 – 80	1.7303	0.4	1.7280	0.7	1.7356	0.6	1.7310	0.3
Evaluation 2								
3 – 5	1.2585	3.8	1.0654	11.	1.1853	5.9	1.2238	3.1
5 – 7.5	1.1343	2.4	1.0919	5.9	1.1586	3.7	1.1361	1.9
7.5 – 10	1.4648	1.9	1.3532	4.4	1.4636	2.8	1.4513	1.5
10 – 12.5	1.2641	1.7	1.2776	3.6	1.3211	2.3	1.2825	1.3
12.5 – 15	1.4439	1.4	1.4403	3.0	1.4911	2.1	1.4562	1.1
15 – 20	1.4966	0.9	1.5320	1.9	1.4966	1.3	1.5018	0.7
20 – 25	1.6458	0.8	1.6321	1.5	1.6654	1.2	1.6493	0.6
25 – 30	1.5759	0.8	1.5858	1.3	1.5775	1.0	1.5781	0.6
30 – 40	1.6702	0.6	1.6439	1.0	1.6573	0.8	1.6617	0.4
40 – 50	1.7875	0.6	1.7563	1.0	1.7658	0.8	1.7760	0.4
50 – 60	1.7210	0.5	1.7365	1.0	1.7305	0.8	1.7260	0.4
60 – 80	1.6992	0.5	1.7301	0.8	1.7244	0.6	1.7114	0.3
80 – 100	1.7023	0.5	1.6770	0.8	1.7173	0.7	1.7020	0.4
100 – 120	1.4724	0.6	1.4925	0.9	1.5163	0.8	1.4890	0.4
120 – 150	–	–	1.3900	0.8	–	–	1.3900	0.8
150 – 175	–	–	1.3138	0.9	–	–	1.3138	0.9
175 – 200	–	–	1.2312	1.1	–	–	1.2312	1.1
200 – 225	–	–	1.1983	1.6	–	–	1.1983	1.6
30 – 80	1.7195	0.4	1.7167	0.5	1.7195	0.5	1.7188	0.3

Table 13: $\sigma(^{161}\mathrm{Dy})/\sigma(^{197}\mathrm{Au})$ AND STATISTICAL UNCERTAINTIES IN (%)

Energy Bin (keV)	Run I		Run II		Run III		Average	
Evaluation 1								
3 – 5	2.9152	5.4	3.4715	13.	3.3278	6.9	3.1128	4.1
5 – 7.5	2.7288	3.0	3.0223	7.6	3.3018	4.4	2.9237	2.4
7.5 – 10	3.7579	2.4	3.0478	5.7	3.8975	3.5	3.7195	1.9
10 – 12.5	3.3194	1.9	3.1451	4.3	3.4005	2.7	3.3239	1.5
12.5 – 15	3.6742	1.6	3.5185	3.7	3.7961	2.3	3.6919	1.2
15 – 20	3.5553	1.0	3.7781	2.2	3.7144	1.4	3.6307	0.8
20 – 25	3.9963	0.9	4.0292	1.8	4.0124	1.2	4.0058	0.7
25 – 30	3.9620	0.8	3.9256	1.5	3.9703	1.1	3.9588	0.6
30 – 40	3.8472	0.6	3.7958	1.1	3.7690	0.8	3.8173	0.4
40 – 50	3.8345	0.6	3.7171	1.1	3.7302	0.9	3.7879	0.4
50 – 60	3.4079	0.6	3.4560	1.1	3.4016	0.8	3.4134	0.4
60 – 80	3.2553	0.5	3.2616	0.9	3.2522	0.7	3.2555	0.4
80 – 100	3.1480	0.5	3.1136	0.9	3.1092	0.8	3.1324	0.4
100 – 120	2.8223	0.6	2.7251	1.0	2.8224	0.9	2.8035	0.4
120 – 150	–	–	2.3710	0.9	–	–	2.3710	0.9
150 – 175	–	–	2.1280	1.0	–	–	2.1280	1.0
175 – 200	–	–	1.9397	1.1	–	–	1.9397	1.1
200 – 225	–	–	1.8473	1.9	–	–	1.8473	1.9
30 – 80	3.5862	0.4	3.5576	0.7	3.5383	0.6	3.5685	0.3
Evaluation 2								
3 – 5	2.9176	3.8	3.2049	9.7	3.2030	5.2	3.0334	2.9
5 – 7.5	2.7735	2.2	2.8864	5.4	3.1375	3.2	2.8889	1.7
7.5 – 10	3.7147	1.8	3.4277	4.2	3.6490	2.6	3.6638	1.4
10 – 12.5	3.3057	1.4	3.2208	3.3	3.3260	2.0	3.3025	1.1
12.5 – 15	3.6198	1.2	3.5616	2.8	3.8499	1.8	3.6792	1.0
15 – 20	3.7043	0.8	3.8758	1.7	3.8812	1.1	3.7791	0.6
20 – 25	4.0165	0.7	4.0775	1.4	4.0259	1.0	4.0284	0.5
25 – 30	3.8649	0.6	3.9267	1.2	3.9157	0.8	3.8897	0.5
30 – 40	3.7974	0.5	3.7730	0.8	3.7582	0.7	3.7819	0.4
40 – 50	3.7521	0.5	3.7026	0.9	3.6893	0.7	3.7268	0.4
50 – 60	3.3481	0.5	3.4324	0.9	3.3744	0.7	3.3681	0.4
60 – 80	3.1813	0.4	3.2599	0.8	3.2293	0.6	3.2069	0.3
80 – 100	3.0811	0.4	3.0922	0.8	3.0715	0.6	3.0804	0.3
100 – 120	2.7471	0.5	2.6971	0.8	2.7878	0.7	2.7477	0.4
120 – 150	–	–	2.3442	0.8	–	–	2.3442	0.8
150 – 175	–	–	2.0988	0.9	–	–	2.0988	0.9
175 – 200	–	–	1.9141	1.0	–	–	1.9141	1.0
200 – 225	–	–	1.8286	1.6	–	–	1.8286	1.6
30 – 80	3.5197	0.3	3.5420	0.5	3.5128	0.5	3.5209	0.2

Table 14: $\sigma(^{162}\mathrm{Dy})/\sigma(^{197}\mathrm{Au})$ AND STATISTICAL UNCERTAINTIES IN (%)

Energy Bin (keV)	Run I		Run II		Run III		Average	
Evaluation 1								
3 – 5	0.4281	6.3	0.3349	19.	0.3728	9.8	0.4066	5.1
5 – 7.5	0.4872	3.0	0.5831	7.0	0.5658	4.6	0.5194	2.4
7.5 – 10	0.6536	2.4	0.5357	5.5	0.6433	3.6	0.6371	1.9
10 – 12.5	0.6372	1.8	0.5609	4.1	0.5965	2.7	0.6176	1.4
12.5 – 15	0.6949	1.5	0.6835	3.4	0.7235	2.2	0.7014	1.2
15 – 20	0.7809	0.9	0.8008	2.0	0.7960	1.4	0.7877	0.7
20 – 25	0.8115	0.8	0.7769	1.6	0.8202	1.2	0.8087	0.6
25 – 30	0.8459	0.7	0.8387	1.3	0.8569	1.0	0.8478	0.5
30 – 40	0.8361	0.5	0.8215	1.0	0.8371	0.8	0.8338	0.4
40 – 50	0.9119	0.6	0.8993	1.0	0.9041	0.8	0.9076	0.4
50 – 60	0.8899	0.5	0.8839	1.0	0.8882	0.8	0.8885	0.4
60 – 80	0.9381	0.5	0.9334	0.8	0.9371	0.7	0.9370	0.3
80 – 100	0.7879	0.5	0.7789	0.8	0.7935	0.7	0.7876	0.4
100 – 120	0.6711	0.6	0.6763	0.9	0.6868	0.8	0.6762	0.4
120 – 150	–	–	0.6161	0.8	–	–	0.6161	0.8
150 – 175	–	–	0.5675	0.9	–	–	0.5675	0.9
175 – 200	–	–	0.5344	1.0	–	–	0.5344	1.0
200 – 225	–	–	0.5318	1.5	–	–	0.5318	1.5
30 – 80	0.8940	0.4	0.8845	0.6	0.8916	0.6	0.8917	0.3
Evaluation 2								
3 – 5	0.4486	4.2	0.4036	12.	0.4095	6.5	0.4346	3.4
5 – 7.5	0.5132	2.1	0.5736	5.0	0.5737	3.2	0.5367	1.7
7.5 – 10	0.6525	1.8	0.6329	4.0	0.6236	2.6	0.6421	1.4
10 – 12.5	0.6231	1.4	0.6149	3.1	0.6178	2.0	0.6206	1.1
12.5 – 15	0.6973	1.2	0.7129	2.5	0.7422	1.7	0.7118	0.9
15 – 20	0.7988	0.8	0.8297	1.5	0.8217	1.1	0.8097	0.6
20 – 25	0.8205	0.7	0.8183	1.3	0.8365	1.0	0.8249	0.5
25 – 30	0.8373	0.6	0.8495	1.1	0.8514	0.8	0.8436	0.5
30 – 40	0.8324	0.5	0.8276	0.8	0.8368	0.6	0.8328	0.3
40 – 50	0.8987	0.5	0.9013	0.8	0.8950	0.7	0.8982	0.4
50 – 60	0.8787	0.5	0.8860	0.8	0.8809	0.7	0.8805	0.3
60 – 80	0.9203	0.4	0.9327	0.7	0.9275	0.6	0.9243	0.3
80 – 100	0.7741	0.4	0.7750	0.7	0.7829	0.6	0.7766	0.3
100 – 120	0.6562	0.5	0.6690	0.8	0.6773	0.7	0.6647	0.4
120 – 150	–	–	0.6096	0.7	–	–	0.6096	0.7
150 – 175	–	–	0.5631	0.8	–	–	0.5631	0.8
175 – 200	–	–	0.5299	0.9	–	–	0.5299	0.9
200 – 225	–	–	0.5269	1.3	–	–	0.5269	1.3
30 – 80	0.8825	0.3	0.8869	0.5	0.8851	0.5	0.8840	0.2

Table 15: $\sigma(^{163}\mathrm{Dy})/\sigma(^{197}\mathrm{Au})$ AND STATISTICAL UNCERTAINTIES IN (%)

Energy Bin (keV)	Run I		Run II		Run III		Average	
Evaluation 1								
3 – 5	1.7396	4.5	1.4218	13.	1.5753	6.6	1.6656	3.6
5 – 7.5	1.6301	2.5	1.5948	6.6	1.7105	4.1	1.6468	2.0
7.5 – 10	1.9191	2.2	1.6864	4.9	1.9301	3.3	1.8926	1.7
10 – 12.5	1.7358	1.7	1.5716	3.9	1.7548	2.5	1.7221	1.3
12.5 – 15	1.8773	1.5	1.7474	3.3	1.9354	2.2	1.8782	1.1
15 – 20	1.9523	0.9	2.0061	2.0	1.9857	1.3	1.9686	0.7
20 – 25	2.1207	0.8	2.0815	1.6	2.0923	1.2	2.1066	0.6
25 – 30	2.1063	0.7	2.1090	1.3	2.1345	1.0	2.1149	0.5
30 – 40	2.0835	0.5	2.0498	0.9	2.0549	0.8	2.0697	0.4
40 – 50	2.1901	0.5	2.1046	1.0	2.1013	0.8	2.1516	0.4
50 – 60	2.1231	0.5	2.1029	1.0	2.0875	0.8	2.1106	0.4
60 – 80	2.0449	0.4	2.0296	0.8	2.0295	0.6	2.0381	0.3
80 – 100	1.9120	0.5	1.8933	0.8	1.8948	0.7	1.9041	0.3
100 – 120	1.7473	0.5	1.7242	0.8	1.7633	0.8	1.7463	0.4
120 – 150	–	–	1.6272	0.8	–	–	1.6272	0.8
150 – 175	–	–	1.5195	0.8	–	–	1.5195	0.8
175 – 200	–	–	1.3922	0.9	–	–	1.3922	0.9
200 – 225	–	–	1.3684	1.4	–	–	1.3684	1.4
30 – 80	2.1104	0.4	2.0717	0.6	2.0683	0.5	2.0925	0.3
Evaluation 2								
3 – 5	1.6613	3.2	1.4635	9.0	1.5308	4.8	1.6084	2.6
5 – 7.5	1.6242	1.8	1.5803	4.6	1.6499	2.9	1.6264	1.5
7.5 – 10	1.8977	1.7	1.7706	3.7	1.8472	2.4	1.8684	1.3
10 – 12.5	1.7428	1.3	1.6413	3.0	1.7079	1.9	1.7214	1.0
12.5 – 15	1.8504	1.1	1.8035	2.5	1.9587	1.7	1.8748	0.9
15 – 20	1.9945	0.7	2.0644	1.5	2.0485	1.1	2.0194	0.6
20 – 25	2.1137	0.7	2.1002	1.3	2.1040	0.9	2.1087	0.5
25 – 30	2.0635	0.6	2.1195	1.0	2.0996	0.8	2.0837	0.4
30 – 40	2.0618	0.5	2.0501	0.8	2.0442	0.6	2.0545	0.3
40 – 50	2.1345	0.5	2.1032	0.8	2.0747	0.6	2.1123	0.3
50 – 60	2.0732	0.4	2.0920	0.8	2.0625	0.6	2.0735	0.3
60 – 80	1.9990	0.4	2.0316	0.7	2.0111	0.5	2.0078	0.3
80 – 100	1.8713	0.4	1.8820	0.7	1.8664	0.5	1.8719	0.3
100 – 120	1.7009	0.5	1.7131	0.7	1.7318	0.6	1.7120	0.3
120 – 150	–	–	1.6056	0.6	–	–	1.6056	0.6
150 – 175	–	–	1.5012	0.7	–	–	1.5012	0.7
175 – 200	–	–	1.3805	0.8	–	–	1.3805	0.8
200 – 225	–	–	1.3471	1.2	–	–	1.3471	1.2
30 – 80	2.0671	0.3	2.0692	0.4	2.0481	0.4	2.0620	0.2

Table 16: $\sigma(^{164}\mathrm{Dy})/\sigma(^{197}\mathrm{Au})$ AND STATISTICAL UNCERTAINTIES IN (%)

Energy Bin (keV)	Run I		Run II		Run III		Average	
Evaluation 1								
3 – 5	0.2677	9.1	0.2121	28.	0.2734	14.	0.2654	7.4
5 – 7.5	0.2857	4.2	0.3492	9.5	0.3396	6.8	0.3068	3.4
7.5 – 10	0.3592	3.3	0.2765	8.2	0.3547	5.4	0.3495	2.6
10 – 12.5	0.3048	2.6	0.2873	6.1	0.3311	4.0	0.3099	2.1
12.5 – 15	0.3710	2.0	0.3603	4.6	0.3837	3.2	0.3729	1.6
15 – 20	0.3909	1.2	0.3882	2.7	0.3972	1.9	0.3922	1.0
20 – 25	0.3881	1.1	0.3759	2.2	0.3920	1.6	0.3874	0.8
25 – 30	0.4170	0.9	0.4143	1.7	0.4282	1.3	0.4197	0.7
30 – 40	0.3959	0.7	0.3963	1.3	0.4067	1.0	0.3989	0.5
40 – 50	0.4257	0.7	0.4307	1.3	0.4276	1.0	0.4270	0.5
50 – 60	0.4265	0.7	0.4209	1.3	0.4288	1.0	0.4263	0.5
60 – 80	0.4165	0.6	0.4199	1.1	0.4296	0.9	0.4204	0.5
80 – 100	0.3201	0.6	0.3177	1.2	0.3268	0.9	0.3214	0.5
100 – 120	0.2532	0.8	0.2569	1.3	0.2660	1.1	0.2573	0.6
120 – 150	–	–	0.2472	1.2	–	–	0.2472	1.2
150 – 175	–	–	0.2142	1.3	–	–	0.2142	1.3
175 – 200	–	–	0.2089	1.4	–	–	0.2089	1.4
200 – 225	–	–	0.2113	2.3	–	–	0.2113	2.3
30 – 80	0.4162	0.5	0.4170	0.9	0.4232	0.8	0.4182	0.4
Evaluation 2								
3 – 5	0.2600	6.8	0.2194	21.	0.2618	11.	0.2575	5.6
5 – 7.5	0.2802	3.3	0.2977	7.8	0.3321	5.0	0.2962	2.6
7.5 – 10	0.3463	2.5	0.3029	6.2	0.3509	3.9	0.3429	2.0
10 – 12.5	0.3120	2.0	0.2999	4.7	0.3327	2.9	0.3165	1.6
12.5 – 15	0.3691	1.6	0.3793	3.4	0.3897	2.4	0.3758	1.2
15 – 20	0.3963	1.0	0.4056	2.1	0.4096	1.5	0.4012	0.8
20 – 25	0.3896	0.9	0.3923	1.7	0.3973	1.3	0.3922	0.7
25 – 30	0.4104	0.8	0.4143	1.4	0.4218	1.0	0.4143	0.6
30 – 40	0.3934	0.6	0.3909	1.1	0.4026	0.8	0.3956	0.4
40 – 50	0.4207	0.6	0.4254	1.1	0.4243	0.8	0.4225	0.4
50 – 60	0.4199	0.6	0.4228	1.1	0.4240	0.8	0.4215	0.4
60 – 80	0.4089	0.5	0.4173	0.9	0.4225	0.7	0.4139	0.4
80 – 100	0.3135	0.5	0.3148	1.0	0.3207	0.8	0.3157	0.4
100 – 120	0.2466	0.7	0.2536	1.1	0.2621	0.9	0.2524	0.5
120 – 150	–	–	0.2436	1.0	–	–	0.2436	1.0
150 – 175	–	–	0.2144	1.1	–	–	0.2144	1.1
175 – 200	–	–	0.2058	1.2	–	–	0.2058	1.2
200 – 225	–	–	0.2108	1.9	–	–	0.2108	1.9
30 – 80	0.4107	0.4	0.4141	0.7	0.4184	0.6	0.4134	0.3

Table 17: $\sigma(^{141}Pr)/\sigma(^{197}Au)$ AND STATISTICAL UNCERTAINTIES IN (%)

Energy Bin (keV)	Run II		Run III		Average	
Evaluation 1						
3 – 5	0.0974	52.	0.1714	19.	0.1630	18.
5 – 7.5	0.2171	13.	0.2361	8.3	0.2305	6.9
7.5 – 10	0.1528	13.	0.1752	8.9	0.1679	7.3
10 – 12.5	0.1652	9.1	0.1973	5.6	0.1884	4.8
12.5 – 15	0.1691	7.9	0.1949	5.0	0.1874	4.2
15 – 20	0.1858	4.4	0.2026	2.9	0.1975	2.4
20 – 25	0.2123	3.2	0.2170	2.4	0.2153	1.9
25 – 30	0.1876	2.8	0.2010	2.0	0.1964	1.7
30 – 40	0.1911	2.0	0.1956	1.6	0.1939	1.3
40 – 50	0.1910	2.0	0.1911	1.6	0.1910	1.3
50 – 60	0.1804	2.1	0.1879	1.6	0.1851	1.3
60 – 80	0.1758	1.8	0.1830	1.4	0.1802	1.1
80 – 100	0.1763	1.7	0.1810	1.4	0.1791	1.1
100 – 120	0.1672	1.8	0.1710	1.6	0.1693	1.2
120 – 150	0.1600	1.7	–	–	0.1600	1.7
150 – 175	0.1222	1.9	–	–	0.1222	1.9
175 – 200	0.1140	2.1	–	–	0.1140	2.1
200 – 225	0.1151	3.5	–	–	0.1151	3.5
30 – 80	0.1846	1.4	0.1894	1.3	0.1876	1.0
Evaluation 2						
3 – 5	0.1601	24.	0.1722	14.	0.1691	12.
5 – 7.5	0.2198	9.0	0.2326	6.1	0.2286	5.1
7.5 – 10	0.1772	8.9	0.1864	6.1	0.1835	5.0
10 – 12.5	0.1880	6.4	0.2174	3.9	0.2096	3.3
12.5 – 15	0.1911	5.4	0.2011	3.8	0.1978	3.1
15 – 20	0.2032	3.2	0.2077	2.3	0.2062	1.8
20 – 25	0.2197	2.5	0.2230	1.8	0.2219	1.5
25 – 30	0.1893	2.2	0.2006	1.6	0.1967	1.3
30 – 40	0.1900	1.6	0.1948	1.2	0.1930	1.0
40 – 50	0.1874	1.7	0.1882	1.3	0.1879	1.0
50 – 60	0.1807	1.7	0.1850	1.2	0.1835	1.0
60 – 80	0.1753	1.4	0.1793	1.1	0.1779	0.9
80 – 100	0.1742	1.4	0.1776	1.1	0.1763	0.9
100 – 120	0.1646	1.4	0.1689	1.2	0.1671	0.9
120 – 150	0.1580	1.3	–	–	0.1580	1.3
150 – 175	0.1214	1.6	–	–	0.1214	1.6
175 – 200	0.1112	1.8	–	–	0.1112	1.8
200 – 225	0.1094	2.9	–	–	0.1094	2.9
30 – 80	0.1834	1.1	0.1868	0.9	0.1856	0.7

Table 18: FINAL NEUTRON CAPTURE CROSS SECTION RATIOS OF ^{160}Dy, ^{161}Dy, ^{162}Dy, ^{163}Dy ^{164}Dy, AND ^{141}Pr RELATIVE TO ^{197}Au

Energy Bin[a]	$\frac{\sigma(^{160}Dy)}{\sigma(^{197}Au)}$	Uncertainty (%)			$\frac{\sigma(^{161}Dy)}{\sigma(^{197}Au)}$	Uncertainty (%)			$\frac{\sigma(^{162}Dy)}{\sigma(^{197}Au)}$	Uncertainty (%)		
(keV)		stat	sys	tot		stat	sys	tot		stat	sys	tot
3 – 5	1.2238	3.1	1.2	3.3	3.0334	2.9	0.9	3.0	0.4346	3.4	0.7	3.5
5 – 7.5	1.1361	1.9	1.2	2.2	2.8889	1.7	0.9	1.9	0.5367	1.7	0.7	1.8
7.5 – 10	1.4513	1.5	1.2	1.9	3.6638	1.4	0.9	1.7	0.6421	1.4	0.7	1.6
10 – 12.5	1.2825	1.3	1.2	1.8	3.3025	1.1	0.9	1.4	0.6206	1.1	0.7	1.3
12.5 – 15	1.4562	1.1	1.2	1.6	3.6792	1.0	0.9	1.3	0.7118	0.9	0.7	1.1
15 – 20	1.5018	0.7	1.2	1.4	3.7791	0.6	0.9	1.1	0.8097	0.6	0.7	0.9
20 – 25	1.6493	0.6	1.2	1.3	4.0284	0.5	0.9	1.0	0.8249	0.5	0.7	0.9
25 – 30	1.5781	0.6	1.2	1.3	3.8897	0.5	0.9	1.0	0.8436	0.5	0.7	0.9
30 – 40	1.6617	0.4	1.2	1.3	3.7819	0.4	0.9	1.0	0.8328	0.3	0.7	0.8
40 – 50	1.7760	0.4	1.2	1.3	3.7268	0.4	0.9	1.0	0.8982	0.4	0.7	0.8
50 – 60	1.7260	0.4	1.2	1.3	3.3681	0.4	0.9	1.0	0.8805	0.3	0.7	0.8
60 – 80	1.7114	0.3	1.2	1.2	3.2069	0.3	0.9	0.9	0.9243	0.3	0.7	0.8
80 – 100	1.7020	0.4	1.2	1.3	3.0804	0.3	0.9	0.9	0.7766	0.3	0.7	0.8
100 – 120	1.4890	0.4	1.2	1.3	2.7477	0.4	0.9	1.0	0.6647	0.4	0.7	0.8
120 – 150	1.3900	0.8	1.2	1.4	2.3442	0.8	0.9	1.2	0.6096	0.7	0.7	1.0
150 – 175	1.3138	0.9	1.2	1.5	2.0988	0.9	0.9	1.3	0.5631	0.8	0.7	1.1
175 – 200	1.2312	1.1	1.2	1.6	1.9141	1.0	0.9	1.3	0.5299	0.9	0.7	1.1
200 – 225	1.1983	1.6	1.2	2.0	1.8286	1.6	0.9	1.8	0.5269	1.3	0.7	1.5

Energy Bin[a]	$\frac{\sigma(^{163}Dy)}{\sigma(^{197}Au)}$	Uncertainty (%)			$\frac{\sigma(^{164}Dy)}{\sigma(^{197}Au)}$	Uncertainty (%)			$\frac{\sigma(^{141}Pr)}{\sigma(^{197}Au)}$	Uncertainty (%)		
(keV)		stat	sys	tot		stat	sys	tot		stat	sys	tot
3 – 5	1.6084	2.6	0.9	2.8	0.2575	5.6	1.3	5.7	0.1691	12.2	0.7	12.2
5 – 7.5	1.6264	1.5	0.9	1.7	0.2962	2.6	1.3	2.9	0.2286	5.1	0.7	5.1
7.5 – 10	1.8684	1.3	0.9	1.6	0.3429	2.0	1.3	2.4	0.1835	5.0	0.7	5.0
10 –12.5	1.7214	1.0	0.9	1.3	0.3165	1.6	1.3	2.1	0.2096	3.3	0.7	3.4
12.5 – 15	1.8748	0.9	0.9	1.3	0.3758	1.2	1.3	1.8	0.1978	3.1	0.7	3.2
15 – 20	2.0194	0.6	0.9	1.1	0.4012	0.8	1.3	1.5	0.2062	1.8	0.7	1.9
20 – 25	2.1087	0.5	0.9	1.0	0.3922	0.7	1.3	1.5	0.2219	1.5	0.7	1.7
25 – 30	2.0837	0.4	0.9	1.0	0.4143	0.6	1.3	1.4	0.1967	1.3	0.7	1.5
30 – 40	2.0545	0.3	0.9	0.9	0.3956	0.4	1.3	1.4	0.1930	1.0	0.7	1.2
40 – 50	2.1123	0.3	0.9	0.9	0.4225	0.4	1.3	1.4	0.1879	1.0	0.7	1.2
50 – 60	2.0735	0.3	0.9	0.9	0.4215	0.4	1.3	1.4	0.1835	1.0	0.7	1.2
60 – 80	2.0078	0.3	0.9	0.9	0.4139	0.4	1.3	1.4	0.1779	0.9	0.7	1.1
80 – 100	1.8719	0.3	0.9	0.9	0.3157	0.4	1.3	1.4	0.1763	0.9	0.7	1.1
100 – 120	1.7120	0.3	0.9	0.9	0.2524	0.5	1.3	1.4	0.1671	0.9	0.7	1.1
120 – 150	1.6056	0.6	0.9	1.1	0.2436	1.0	1.3	1.6	0.1580	1.3	0.7	1.5
150 – 175	1.5012	0.7	0.9	1.1	0.2144	1.1	1.3	1.7	0.1214	1.6	0.7	1.7
175 – 200	1.3805	0.8	0.9	1.2	0.2058	1.2	1.3	1.8	0.1112	1.8	0.7	1.9
200 – 225	1.3471	1.2	0.9	1.5	0.2108	1.9	1.3	2.3	0.1094	2.9	0.7	3.0

[a] Energy bins as used for calculating the Maxwellian averaged cross sections

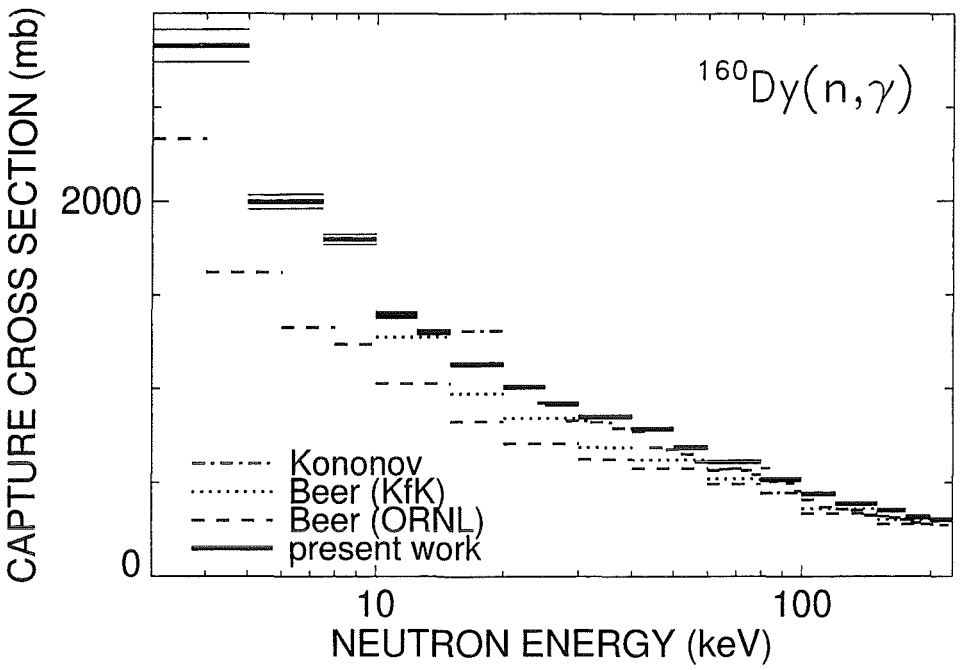

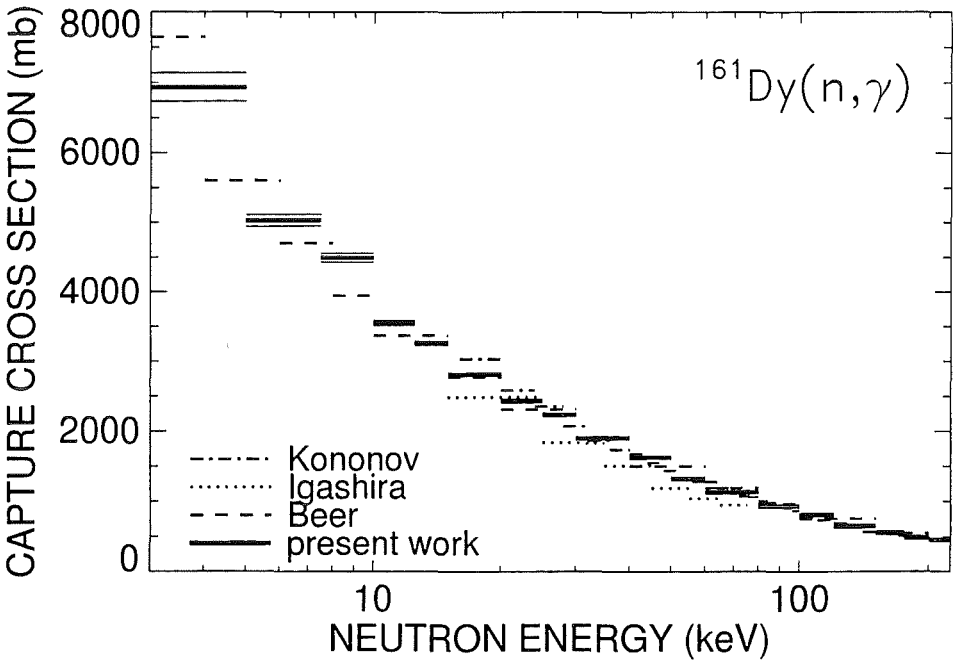

Figure 15: The neutron capture cross sections of ^{160}Dy and ^{161}Dy compared to previous data [30, 31, 33].

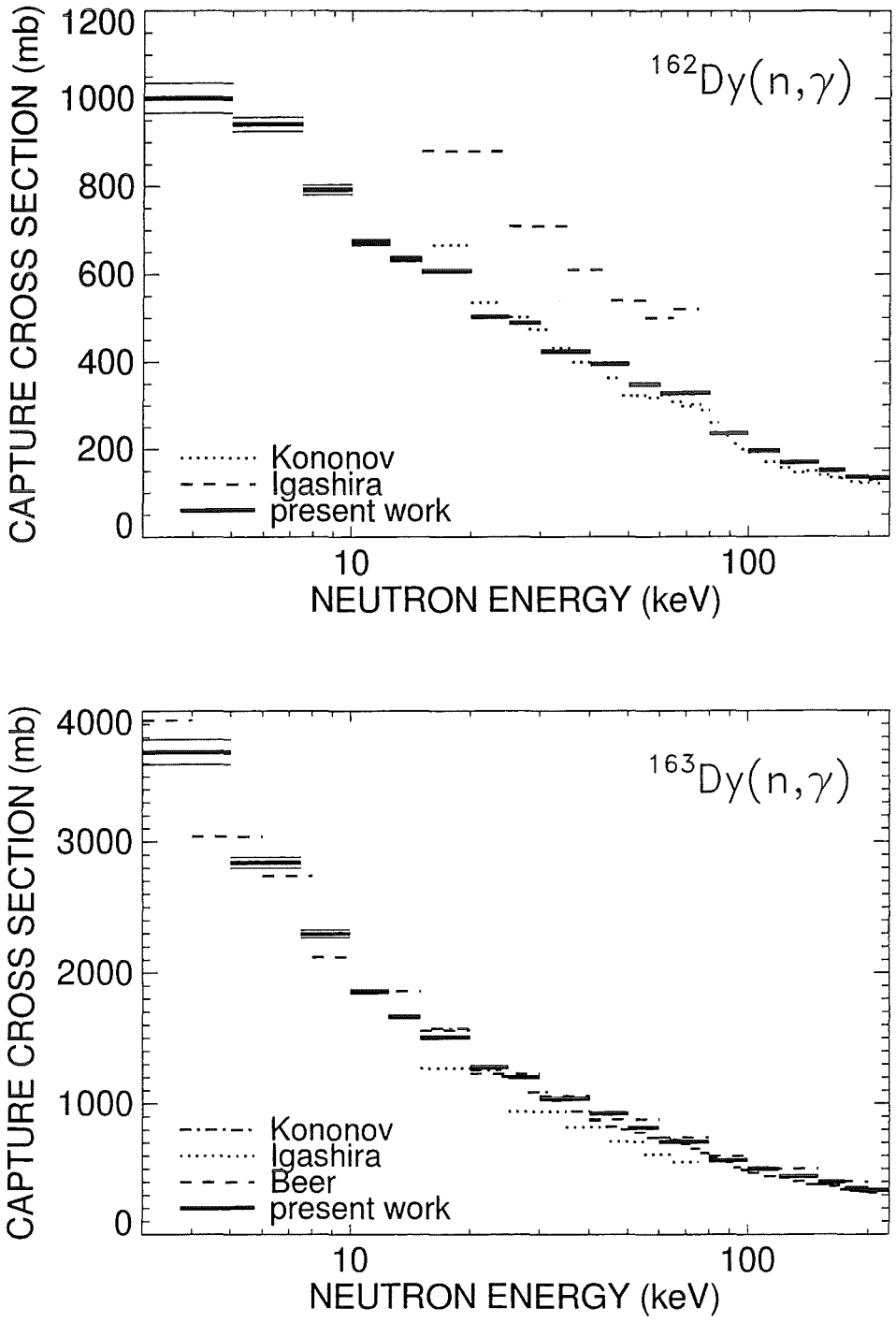

Figure 16: The neutron capture cross sections of ^{162}Dy and ^{163}Dy compared to previous data [30, 32, 33].

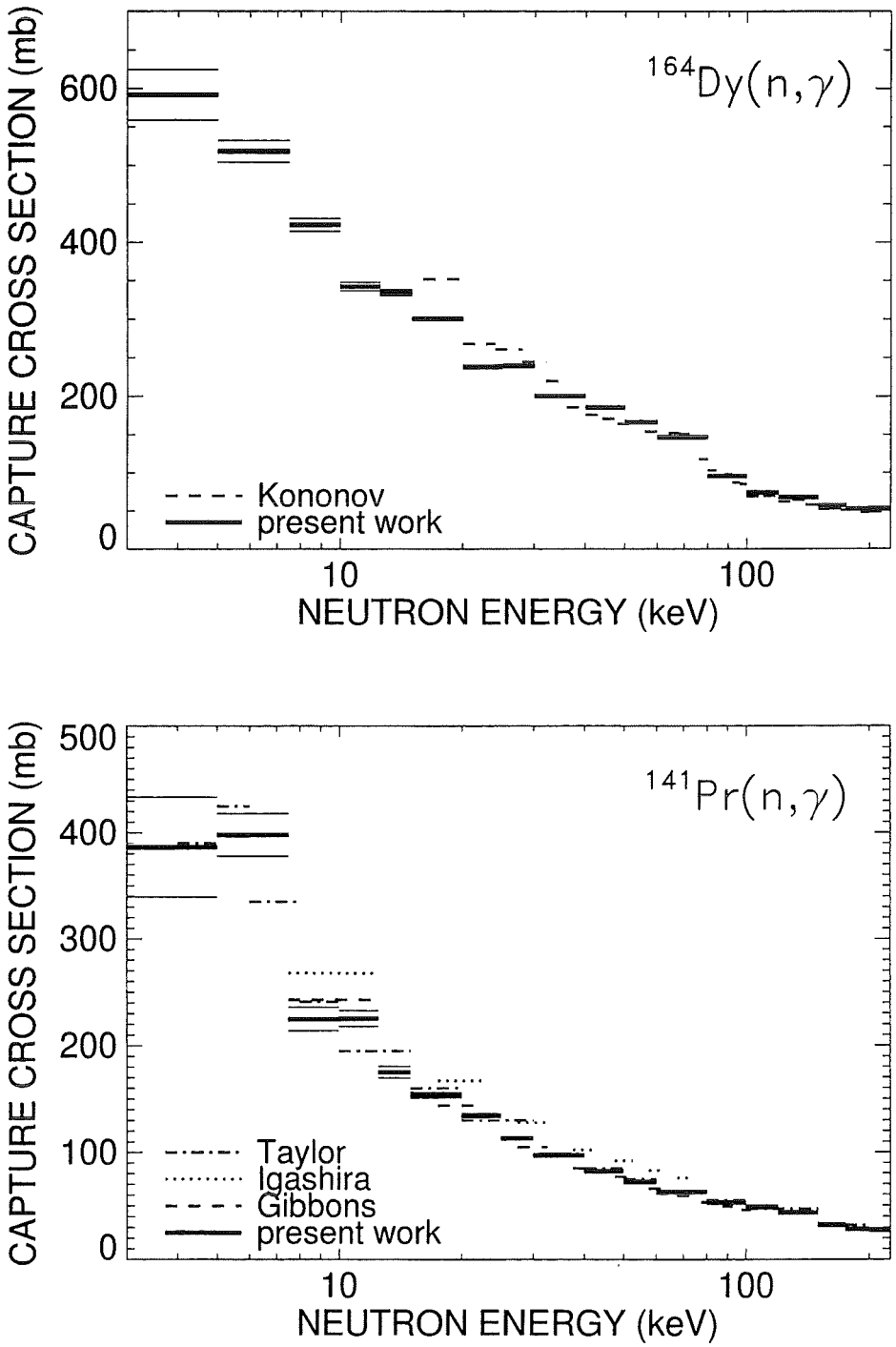

Figure 17: The neutron capture cross sections of ^{164}Dy and ^{141}Pr compared to previous data [30, 34, 35, 36].

Table 19: NEUTRON CAPTURE CROSS SECTIONS OF ^{160}Dy, ^{161}Dy,^{162}Dy, ^{163}Dy, ^{164}Dy, AND ^{141}Pr (in mb).

Energy Bin[a] (keV)	$\sigma(^{197}\mathrm{Au})^b$	$\sigma(^{160}\mathrm{Dy})$	$\sigma(^{161}\mathrm{Dy})$	$\sigma(^{162}\mathrm{Dy})$	$\sigma(^{163}\mathrm{Dy})$	$\sigma(^{164}\mathrm{Dy})$	$\sigma(^{141}\mathrm{Pr})$
3 – 5	2266.7	2774.	6876.	985.1	3646.	583.8	383.3
5 – 7.5	1726.7	1962.	4988.	926.7	2808.	511.4	394.7
7.5 – 10	1215.7	1764.	4454.	780.7	2272.	416.9	223.1
10 – 12.5	1066.7	1368.	3523.	662.0	1836.	337.6	223.6
12.5 – 15	878.0	1279.	3230.	624.9	1646.	330.0	173.7
15 – 20	738.8	1109.	2792.	598.2	1492.	296.4	152.3
20 – 25	600.0	989.6	2417.	495.0	1265.	235.3	133.1
25 – 30	570.8	900.9	2220.	481.5	1189.	236.5	112.3
30 – 40	500.4	831.5	1892.	416.7	1028.	198.0	96.6
40 – 50	433.3	769.6	1615.	389.2	915.3	183.1	81.4
50 – 60	389.6	672.5	1312.	343.1	807.9	164.2	71.5
60 – 80	349.4	597.9	1120.	322.9	701.5	144.6	62.2
80 – 100	298.3	507.7	918.9	231.7	558.4	94.2	52.6
100 – 120	290.1	432.0	797.2	192.9	496.7	73.2	48.5
120 – 150	274.1	381.1	642.6	167.1	440.1	66.8	43.3
150 – 175	263.7	346.4	553.4	148.5	395.8	56.5	32.0
175 – 200	252.6	311.0	483.4	133.8	348.7	52.0	28.1
200 – 225	248.5	297.7	454.3	130.9	334.7	52.4	27.2

[a] As used for calculating the Maxwellian averaged cross sections
[b] Based on the ^{197}Au data from literature[28, 29]

5 DISCUSSION OF UNCERTAINTIES

The determination of statistical and systematic uncertainties in measurements with the 4π BaF_2 detector has been described in Refs. [1, 12, 14]. The following discussion concentrates on the particular aspects of the present experiment. The various uncertainties are compiled in Table 20.

The binding energy for all investigated isotopes is sufficiently low for normalizing the scattering background in the sum energy region around 9 MeV. Therefore, no systematic differences were observed in the data, neither between individual runs nor correlated with the different acquisition modes, evaluation methods or scattering samples (see Tables 12 to 17). This emplies that systematic uncertainties in background subtraction were negligible as in the measurements on the samarium [1] and gadolinium [2] isotopes. This result could be confirmed via the pulse height spectra measured at low neutron energies. The absence of any (positive or negative) structure around 9 MeV γ–ray energy due to

neutron captures in the odd barium isotopes verifies the correct treatment of the scattering background.

The systematic uncertainties due to the flightpath and the neutron flux normalization have been discussed previously and are given in Table 20.

The measured stoichiometry of the praseodymium sample was $PrO_{1.94\pm0.03}$. This uncertainty translates into an uncertainty of 0.3% in the sample mass.

The problem of admixtures of other rare earth elements and especially of europium with its very high cross section has been discussed in detail for ^{142}Nd and ^{144}Nd [37]. Since this background concerns isotopes with small cross sections, it has to be considered mainly for ^{164}Dy. For this sample, impurities of Sm(0.05%), Eu(0.05%), Gd(0.1%), Tb(0.1%), Ho(0.03%), and Er(0.08%) are specified by the supplier. If one takes into account, that the odd impurity isotopes have higher binding energies than ^{164}Dy, this background can be partly discriminated, leaving a correction of 1.1%. In case of the neodymium isotopes [37] detailed neutron activation analyses showed, however, that the actual impurities were significantly smaller, and that the quoted values have to be regarded as upper limits. Therefore, it was renounced to repeat this analysis in the present case. Instead, a systematic uncertainty of 1% was assumed for this uncorrected background.

In the ^{162}Dy sample only impurities of Gd(0.1%), Ho(0.1%), and Er(0.01%) were specified, resulting in a corresponding uncertainty well below 0.2%. This value was adopted for all other isotopes. For the praseodymium sample, elemental oxyde with a purity of 99.999% was used. Contaminations by other elements were specified at the ppm level without any detectable rare earth components. Accordingly, the related uncertainty is negligible.

The isotopic composition (Table 2) was specified with an absolute uncertainty of $<0.2\%$ for the main isotope and $<0.1\%$ for the impurity isotopes in each sample. In view of the very good agreement with the independently measured isotopic composition of the neodymium samples [3] these seem to be rather conservative estimates. Nevertheless, this information was adopted in the analysis, resulting in a relative uncertainty of 0.2% for the mass of the main isotopes in the enriched samples. For the less enriched ^{160}Dy sample, however, an uncertainty of 0.5% had to be assumed instead.

The uncertainty of the isotopic correction can directly be evaluated from the spectra shown in the upper part of Fig. 5. In case of the ^{160}Dy sample, the count rate between threshold and channel 68, which is used for determining the cross section, consists of contributions from captures in ^{160}Dy (44%), ^{162}Dy (7%), and ^{161}Dy (49%). The abundances of ^{161}Dy and ^{162}Dy are $34.4\pm0.1\%$ and $13.4\pm0.1\%$, respectively. This implies, that the ^{161}Dy and ^{162}Dy components carry relative systematic uncertainties of 0.3% and 0.7%, resulting in a systematic uncertainty of 0.4% for the remaining count rate of ^{160}Dy after correction. For all other isotopes the isotopic corrections are much smaller with corresponding uncertainties of 0.2%.

Samples with low enrichment are also problematic with respect to the correction for multiple scattering and self–shielding. Subtraction of the normalized spectra of the impurity isotopes may either be insufficient or may even overcompensate the multiple scattering effect. This holds certainly if the individual sample masses are significantly different as it was the case for the ^{160}Dy and ^{161}Dy samples compared to the ^{164}Dy and ^{163}Dy samples. Accordingly, the overcompensation was clearly visible in the sum energy spectra and re-

Table 20: SYSTEMATIC UNCERTAINTIES (%)

Flight path	0.1
Neutron flux normalization	0.2
Stoichiometry of the ^{141}Pr sample	0.3
Sample mass: elemental impurities (^{164}Dy/other Dy samples)	1.0/0.2
Isotopic composition (^{160}Dy/other Dy samples)	0.5/0.2
Isotopic correction (^{160}Dy/other Dy samples)	0.4/0.2
Multiple scattering and self-shielding: F_2	
cross section ratio (^{160}Dy/^{164}Dy/others)	0.9/0.7/0.4
Undetected events: F_1	
cross section ratio (even Dy and Pr/odd Dy)	0.4/0.7
total systematic uncertainties	
$\sigma(^{160}\mathrm{Dy})/\sigma(\mathrm{Au})$	1.2
$\sigma(^{161}\mathrm{Dy})/\sigma(\mathrm{Au})$	0.9
$\sigma(^{162}\mathrm{Dy})/\sigma(\mathrm{Au})$	0.7
$\sigma(^{163}\mathrm{Dy})/\sigma(\mathrm{Au})$	0.9
$\sigma(^{164}\mathrm{Dy})/\sigma(\mathrm{Au})$	1.3
$\sigma(^{141}\mathrm{Pr})/\sigma(\mathrm{Au})$	0.7

quired the renormalization of this correction (Sec. 3). For all other samples the effect was not visible in the spectra but may still cause a small uncertainty. Therefore, the calculation of the correction factors MS were performed twice, before and after the correction for isotopic impurities. The respective differences were 2.1% for the ^{160}Dy sample, 1.4% for the ^{164}Dy sample, and less than 0.4% in all other cases, nearly independent of neutron energy. In analogy to the gadolinium experiment [2], 25% of this difference were adopted as the related systematic uncertainty and were added to the uncertainties provided by the SESH code [17].

The systematic uncertainties due to undetected events were discussed in detail for the gadolinium experiment [2], where uncertainties of 0.3% for the even and 0.8% for the odd isotopes were estimated for the correction factor F_1. This estimate was based on two independent sets of calculated capture cascades, and was found to agree with the respective uncertainties quoted in previous measurements with the 4π BaF_2 detector [1, 12, 27]. It turned out that this uncertainty was mainly determined by the difference in binding energy between the investigated isotope and the gold standard, which is large for the odd, but small for the even gadolinium isotopes. For dysprosium the same effect is observed but the differences are slightly larger for the even and lower for the odd isotopes, but with different signs for odd and even nuclei. Therefore, uncertainties of 0.4% and 0.7% had to be assigned, respectively. Since the neutron magic nucleus ^{141}Pr has a low binding energy, similar to that of the even Dy isotopes, an 0.4% uncertainty was assigned to this isotope as well.

6 MAXWELLIAN AVERAGED CROSS SECTIONS

Maxwellian averaged cross sections were calculated in the same way as described in Refs. [12, 14]. The neutron energy range from 0 to 700 keV was divided into three intervals according to the origin of the adopted cross sections. The respective contributions I_x are given in Table 21. The main contribution, i.e. the interval I_2 from 3 to 225 keV, is provided by the results of the present experiment (Table 19). These data were obtained with sufficient resolution to exclude systematic uncertainties that may be caused from a coarse energy grid.

As in previous work, the contribution I_1 was determined in two ways. First, the cross sections were calculated from resonance parameters [26] and normalized to the results of the present experiment. For the three isotopes ^{162}Dy, ^{164}Dy, and ^{141}Pr resonance parameters were available in the entire interval from 0 to 3 keV, while only restricted data up to 1 or 2 keV were known for the other isotopes. In these cases, the remaining gap was covered by a statistical model calculation.

In the second approach the cross sections of the JEF file [18] were normalized to the present data between 5 to 20 keV. However, for most of the isotopes of the present study the cross section shape as well as the absolute values were found to differ completely from the measured data. Under these circumstances, a reliable normalization was only possible for ^{164}Dy and ^{141}Pr. It turned out that the JEF file is identical with the ENDF/B-VI evaluation [38], where these cross sections have been adopted unchanged from the 1973 ENDF/B-III version. The poor quality of these data is illustrated in Ref. [22], where the ^{164}Dy cross section is determined by fitting experimental data measured in 1959. In view of this unsatisfactory situation only the results of the first calculation were considered. The quoted uncertainties of 10% include the respective systematic uncertainties for this interval. For the two isotopes, where the JEF data could be normalized, the results of both calculations agreed to better than 5%.

The energy interval from 225 to 700 keV contributes very little to the Maxwellian average at typical *s*-process temperatures. Here the data of Kononov *et al.* [30] were used up to 460 keV neutron energy, normalized to the present results in the energy range from 100 to 225 keV, and in the remaining gap the shape from the JEF-evaluation was used. The uncertainties were calculated under the assumption that the uncertainties of the normalized cross sections increased from 2% at 225 keV to 10% at 700 keV neutron energy.

The systematic uncertainties of the Maxwellian averaged cross sections in Table 21 correspond to the uncertainties of the cross section ratios (Table 18) and consider the I_1 and I_3 contributions. The 1.5% uncertainty of the gold standard was not included since it cancels out in most applications of relevance for *s*-process studies. In general, the systematic uncertainties dominate over the statistical uncertainties, except at low thermal energies.

The present results at kT=30 keV are eventually compared in Table 22 with previous

experiments and with the compilations of Bao and Käppeler [39] and Beer, Voss, and Winters [40]. For the calculation of the Maxwellian average the data of Kononov *et al.* [30] (see Figs. 15 to 17) were corrected by a factor of 0.927 to compensate for the different gold cross section [41]. Overall, good agreement is found compared to previous experiments. The largest discrepancies of 20 to 30% were obtained for the *s*–only isotope ^{160}Dy, which bear important astrophysical consequences. Differences of 15 to 20% are also found with respect to the results of Kononov *et al.* for ^{163}Dy and ^{164}Dy. Naturally, these differences show also up in the evaluations for ^{160}Dy and ^{164}Dy. The data of Kononov *et al.* [30] have been reanalyzed and new Maxwellian averaged cross sections were published in Ref. [42] which agree to the present data within 10% for all isotopes. The present results for ^{141}Pr are ~15% higher compared to the calculated cross section that was used in a recent evaluation of the *s* process in the region of the neodymium isotopes [43].

Table 21: MAXWELLIAN AVERAGED NEUTRON CAPTURE CROSS SECTIONS OF ^{141}Pr AND OF THE DYSPROSIUM ISOTOPES.

			^{160}Dy				
ΔE	0 - 3 keV	3 - 225 keV	225 - 700 keV	Thermal Spectrum			
Data:	see text	this work	from Ref. [30][a]				
kT	I_1	I_2	I_3	$<\sigma v>/v_T$ (mbarn)			
(keV)	(mbarn)	(mbarn)	(mbarn)		stat	sys[b]	tot
10	194.5±19.	1383.±8.2	0.0	1578.	21.	17.	27.
12	138.9±14.	1291.±6.7	0.0	1430.	16.	16.	23.
20	52.8±5.3	1043.±3.9	0.0	1096.	6.6	13.	15.
25	34.4±3.4	943.0±3.1	0.4	977.8	4.6	12.	13.
30	24.2±2.4	864.1±2.7	1.4	889.7	3.6	11.	12.
40	13.7±1.4	743.3±2.2	7.0±0.2	764.0	2.6	9.2	9.6
50	8.9±0.9	650.5±1.9	17.9±0.5	677.3	2.2	8.2	8.5
52	8.2±0.8	634.2±1.9	20.5±0.6	662.9	2.2	8.0	8.3
60	6.2±0.6	574.4±1.7	32.4±1.1	613.0	2.1	7.4	7.7
70	4.6±0.5	510.2±1.6	48.9±1.7	563.7	2.4	6.8	7.2
80	3.5±0.4	455.3±1.5	65.5±2.4	524.3	2.9	6.4	7.0
90	2.8±0.3	408.1±1.3	81.2±3.1	492.1	3.4	6.0	6.9
100	2.3±0.2	367.3±1.3	95.6±3.9	465.2	4.1	5.7	7.0
			^{161}Dy				
ΔE	0 - 3 keV	3 - 225 keV	225 - 700 keV	Thermal Spectrum			
Data:	see text	this work	from Ref. [30][a]				
kT	I_1	I_2	I_3	$<\sigma v>/v_T$ (mbarn)			
(keV)	(mbarn)	(mbarn)	(mbarn)		stat	sys[b]	tot
10	474.6±47.	3416.±19.	0.0	3891.	51.	31.	60.
12	339.1±34.	3152.±15.	0.0	3491.	37.	29.	47.
20	129.4±13.	2424.±8.4	0.1	2554.	15.	22.	27.
25	84.2±8.4	2129.±6.6	0.5	2214.	11.	19.	22.
30	59.2±5.9	1903.±5.5	1.9	1964.	8.1	17.	19.
40	33.8±3.4	1572.±4.2	9.5±0.3	1615.	5.4	14.	15.

Table 21 (continued)

50	21.8±2.2	1334.±3.5	24.1±0.7	1380.	4.2	12.	13.
52	20.2±2.0	1294.±3.4	27.7±0.8	1342.	4.0	12.	13.
60	15.3±1.5	1151.±3.1	43.4±1.4	1210.	3.7	11.	12.
70	11.2±1.1	1004.±2.7	64.5±2.1	1080.	3.6	9.7	10.
80	8.6±0.9	883.6±2.5	85.1±3.0	977.3	4.0	8.8	9.7
90	6.8±0.7	783.1±2.2	104.2±3.8	894.1	4.4	8.0	9.1
100	5.6±0.6	698.4±2.0	120.9±4.6	824.9	5.1	7.4	9.0

^{162}Dy

ΔE	0 - 3 keV	3 - 225 keV	225 - 700 keV	Thermal Spectrum			
Data:	see text	this work	from Ref. [30][a]				
kT	I_1	I_2	I_3	$<\sigma v>/v_T$ (mbarn)			
(keV)	(mbarn)	(mbarn)	(mbarn)		stat	sys[b]	tot
10	136.4±14.	659.2±3.3	0.0	795.6	14.	4.7	15.
12	97.2±9.7	623.5±2.7	0.0	720.7	10.	4.4	11.
20	36.9±3.7	516.4±1.6	0.0	553.3	4.0	3.7	5.4
25	24.0±2.4	468.2±1.4	0.2	492.4	2.8	3.3	4.3
30	16.8±1.7	428.6±1.2	0.6	446.0	2.1	3.1	3.7
40	9.6±1.0	366.1±0.9	3.1±0.1	378.8	1.3	2.6	2.9
50	6.2±0.6	317.6±0.8	8.0±0.2	331.8	1.0	2.3	2.5
52	5.7±0.6	309.0±0.8	9.2±0.3	323.9	1.0	2.3	2.5
60	4.3±0.4	278.1±0.7	14.6±0.5	297.0	0.9	2.1	2.3
70	3.1±0.3	245.3±0.7	22.0±0.8	270.4	1.1	1.9	2.2
80	2.5±0.3	217.7±0.6	29.5±1.1	249.7	1.3	1.8	2.2
90	2.0±0.2	194.2±0.6	36.7±1.4	232.9	1.5	1.6	2.2
100	1.6±0.2	174.1±0.5	43.2±1.7	218.9	1.8	1.5	2.3

^{163}Dy

ΔE	0 - 3 keV	3 - 225 keV	225 - 700 keV	Thermal Spectrum			
Data:	see text	this work	from Ref. [30][a]				
kT	I_1	I_2	I_3	$<\sigma v>/v_T$ (mbarn)			
(keV)	(mbarn)	(mbarn)	(mbarn)		stat	sys[b]	tot
10	311.8±31.	1820.±9.0	0.0	2132.	32.	17.	36.
12	222.4±22.	1686.±7.2	0.0	1908.	23.	15.	27.
20	84.5±8.5	1327.±4.1	0.1	1412.	9.4	12.	15.
25	55.0±5.5	1183.±3.3	0.4	1238.	6.4	11.	13.
30	38.6±3.9	1072.±2.8	1.5	1112.	4.8	9.7	11.
40	22.1±2.2	906.6±2.2	7.1±0.2	935.8	3.1	8.3	8.9
50	14.3±1.4	784.5±1.8	17.8±0.5	816.6	2.3	7.3	7.7
52	13.2±1.3	763.4±1.8	20.5±0.6	797.1	2.3	7.1	7.5
60	9.9±1.0	687.2±1.6	31.7±1.0	728.8	2.1	6.5	6.8
70	7.3±0.7	606.9±1.5	46.6±1.5	660.8	2.2	5.9	6.3
80	5.6±0.6	539.2±1.3	61.1±2.1	605.9	2.5	5.5	6.0
90	4.5±0.5	481.7±1.2	74.3±2.6	560.5	2.9	5.1	5.9
100	3.7±0.4	432.4±1.1	85.6±3.1	521.7	3.3	4.7	5.7

Table 21 (continued)

^{164}Dy							
ΔE	0 - 3 keV	3 - 225 keV	225 - 700 keV	Thermal Spectrum			
Data:	see text	this work	from Ref. [30][a]				
kT	I_1	I_2	I_3	$<\sigma v>/v_T$ (mbarn)			
(keV)	(mbarn)	(mbarn)	(mbarn)		stat	sys[b]	tot
10	65.1±6.5	339.9±2.9	0.0	405.0	7.2	4.5	8.5
12	46.4±4.6	317.5±2.3	0.0	363.9	5.1	4.2	6.6
20	17.6±1.8	253.5±1.2	0.0	271.1	2.2	3.3	4.0
25	11.5±1.2	225.8±1.0	0.1	237.4	1.6	3.0	3.4
30	8.1±0.8	203.6±0.8	0.2	211.9	1.1	2.7	2.9
40	4.6±0.5	169.5±0.6	1.3	175.4	0.8	2.2	2.3
50	3.0±0.3	144.3±0.5	3.2±0.1	150.5	0.6	1.9	2.0
52	2.8±0.3	140.0±0.5	3.7±0.1	146.5	0.6	1.9	2.0
60	2.1±0.2	124.6±0.4	5.9±0.2	132.6	0.5	1.7	1.8
70	1.6±0.2	108.6±0.4	8.9±0.3	119.1	0.5	1.5	1.6
80	1.2±0.1	95.6±0.4	11.8±0.4	108.6	0.6	1.4	1.5
90	0.9±0.1	84.7±0.3	14.7±0.6	100.3	0.7	1.3	1.5
100	0.8±0.1	75.5±0.3	17.3±0.7	93.6	0.8	1.2	1.4
^{141}Pr							
ΔE	0 - 3 keV	3 - 225 keV	225 - 700 keV	Thermal Spectrum			
Data:	see text	this work	from Ref. [18][a]				
kT	I_1	I_2	I_3	$<\sigma v>/v_T$ (mbarn)			
(keV)	(mbarn)	(mbarn)	(mbarn)		stat	sys[b]	tot
10	49.0±4.9	197.5±4.0	0.0	246.5	6.3	1.4	6.5
12	34.9±3.5	179.8±3.1	0.0	214.7	4.7	1.3	4.9
20	13.2±1.3	134.6±1.6	0.0	147.8	2.1	0.9	2.3
25	8.6±0.9	117.7±1.2	0.0	126.3	1.5	0.8	1.7
30	6.1±0.6	105.2±1.0	0.1	111.4	1.2	0.7	1.4
40	3.5±0.4	87.4±0.7	0.6	91.5	0.8	0.6	1.0
50	2.2±0.2	74.7±0.6	1.4	78.3	0.6	0.5	0.8
52	2.1±0.2	72.5±0.6	1.6±0.1	76.2	0.6	0.5	0.8
60	1.6±0.2	64.9±0.5	2.5±0.1	69.0	0.5	0.5	0.7
70	1.2±0.1	56.9±0.4	3.7±0.1	61.8	0.4	0.4	0.6
80	0.9±0.1	50.3±0.4	5.0±0.2	56.2	0.5	0.4	0.6
90	0.7±0.1	44.7±0.4	6.1±0.2	51.5	0.5	0.4	0.6
100	0.6±0.1	40.0±0.3	7.0±0.3	47.6	0.4	0.3	0.5

[a]Normalized to present data

[b]The 1.5% uncertainty of the gold standard is not included here, since it cancels out in most applications of relevance for nuclear astrophysics

Table 22: MAXWELLIAN AVERAGED CROSS SECTIONS AT kT=30 keV COMPARED TO PREVIOUS EXPERIMENTS AND EVALUATIONS

Isotope	Experiment		Evaluation	
	Cross section (mb)	Reference	Bao and Käppeler [39]	Beer, Voss, Winters [40]
^{160}Dy	889.7 ± 12.	present work[a]	738±35	772±39
	699 ± 35	Beer *et al.* ORELA [31]		
	769 ± 39	Beer *et al.* KfK [31]		
	1077 ± 107	Kononov *et al.* [b] [30]		
	806 ± 40	Bokhovko *et al.* [42]		
^{161}Dy	1964. ± 19.	present work[a]	2007±72	2006±60
	1936 ± 88	Beer *et al.* ORELA [31]		
	2056 ± 74	Beer *et al.* KfK [31]		
	1772 ± 180	Kononov *et al.* [b] [30]		
	1836 ± 92	Bokhovko *et al.* [42]		
^{162}Dy	446.0 ± 3.7	present work[a]	473 ±50	473 ±50
	441±44	Kononov *et al.* [b] [30]		
	427 ± 21	Bokhovko *et al.* [42]		
^{163}Dy	1112. ± 11.	present work[a]	1142±44	1140 ± 38
	1153 ±44	Beer *et al.* ORELA [32]		
	1052 ± 42	Beer *et al.* KfK [32]		
	934 ± 94	Kononov *et al.* [b] [30]		
	1026 ± 51	Bokhovko *et al.* [42]		
^{164}Dy	211.9 ± 2.9	present work[a]	268 ± 27	268 ± 27
	248 ±25	Kononov *et al.* [b] [30]		
	209 ± 15	Bokhovko *et al.* [42]		
^{141}Pr	111.4± 1.4	present work[a]	119 ± 15	119 ± 15
	119 ±15	Taylor *et al.* [34]		

[a] The 1.5% uncertainty of the gold cross section is not included, since it cancels out in most applications of relevance for nuclear astrophysics.
[b] These data have been normalized by a factor of 0.927 to compensate for the different gold cross section.

References

[1] K. Wisshak, K. Guber, F. Voss, F. Käppeler, and G. Reffo, Phys. Rev. C **48**, 1401 (1993).

[2] K. Wisshak, F. Voss, F. Käppeler, K. Guber, L. Kazakov, N. Kornilov, M. Uhl, and G. Reffo, Phys. Rev. C. **52**, 2762 (1995).

[3] K. Wisshak, F. Voss, F. Käppeler, L. Kazakov, and G. Reffo, Phys. Rev. C. **57**, 391 (1998).

[4] E. Anders and N. Grevesse, Geochim. Cosmochim. Acta **53**, 197 (1989).

[5] M.J. Harris, Astrophys. and Space Science **77**, 357 (1981).

[6] J.A. Holmes, S.E. Woosley, W.A. Fowler, and B.A. Zimmerman, Atomic Data and Nucl. Data Tables **18**, 305 (1976).

[7] K. Takahashi, R.N. Boyd, G.J. Mathews, and K. Yokoi, Phys. Rev. C. **36**, 1522 (1987).

[8] M. Jung *et al.* , Phys. Rev. Lett. **69**, 2164 (1992).

[9] S. Jaag and F. Käppeler, Astrophys. J. **464**, 874 (1996).

[10] S. Richter, U. Ott, and F. Begemann, in *Heavy Element Nucleosynthesis*, edited by E. Somorjai and Zs. Fülöp, (Hung. Acad. of Sci., Budapest, 1994), p. 44.

[11] R. Surman, J. Engel, J.R. Bennett, and B.S. Meyer, Phys. Rev. Lett. **79**, 1809 (1997).

[12] K. Wisshak, F. Voss, F. Käppeler, and G. Reffo, Phys. Rev. C **45**, 2470 (1992).

[13] K. Wisshak, K. Guber, F. Käppeler, J. Krisch, H. Müller, G. Rupp, and F. Voss, Nucl. Instr. Meth. A **292**, 595 (1990).

[14] K. Wisshak, F. Voss, F. Käppeler, and G. Reffo, Phys. Rev. C **42**, 1731 (1990).

[15] H. Ottmar, H. Eberle, L. Koch, R. de Meester, and E. Kuhn, in *Nuclear Material Safegards* (International Atomic Energy Agency, Vienna, 1987), p. 201.

[16] R. de Meester, H. Eberle, S. Johnston, L. Koch, I. Michel–Piper, H. Nackaerts, and H. Ottmar, in *Nuclear Material Safegards* (International Atomic Energy Agency, Vienna, 1987), p. 233.

[17] F. H. Fröhner, Technical report, Gulf General Atomic (unpublished).

[18] C. Nordborg, H. Gruppelaar, and M. Salvatores, in *Nuclear Data for Science and Technology*, edited by S. Qaim (Springer, Berlin, 1992), p. 782.

[19] K. Wisshak, F. Voss, Ch. Theis, F. Käppeler, K. Guber, L.Kazakov, N. Kornilov, and G. Reffo, Phys. Rev. C **54**, 1451 (1996).

[20] D.J. Horen, C.H. Johnson, J.L. Fowler, A.D. MacKellar, and B. Castel, Phys. Rev. C **34**, 429 (1986).

[21] J. Schmiedmayer, P. Riehs, J.A. Harvey, and N.W. Hill, in *Nuclear Data for Science and Technology*, edited by S. Qaim (Springer, Berlin, 1992), p. 163.

[22] V. McLane, C.L. Dunford, and P.F. Rose, in *Neutron Cross Sections, Vol. 2,* (Academic Press, New York, 1988).

[23] G. Reffo, F. Fabbri, K. Wisshak, and F. Käppeler, Nucl. Sci. Eng. **80**, 630 (1982).

[24] M. Uhl and J. Kopecky, in *Nuclei in the Cosmos* , edited by F. Käppeler and K. Wisshak (IOP Publishing, Bristol, 1993), p. 259.

[25] A. Gilbert and A.G.W. Cameron, Can. J. Phys. **43**, 1446 (1965).

[26] J. F. Mughabghab, M. Divadeenam, and N. E. Holden, in *Neutron Cross Sections, Vol. 1, Part A* (Academic Press, New York, 1981).

[27] F. Voss, K. Wisshak, K. Guber, F.Käppeler, and G. Reffo, Phys. Rev. C **50**, 2582 (1994).

[28] R. L. Macklin, private communication (unpublished).

[29] W. Ratynski and F. Käppeler, Phys. Rev. C **37**, 595 (1988).

[30] M.V. Bokhovko, L.E. Kazakov, V.N. Kononov, E.D. Poletaev, and V.M. Timokov, Yadernie Const. **4**, 8 (1988).

[31] H. Beer, G. Walter, R.L. Macklin, and P.J. Patchett, Phys. Rev. C **30**, 464 (1984).

[32] H. Beer, G. Walter, R.L. Macklin, in *Capture Gamma-Ray Spectroscopy and Related Topics 1984*, edited by S. Raman, American Inst. of Physics, Conf. Proceedings Nr. 125 (AIP, New York, 1985), p. 778.

[33] M. Igashira, in *1994 Symp. on Nuclear Data*, Report JAERI-Conf 95-008 (Japan Atomic Energy Research Institute, Tokai-Mura, 1995), p. 129.

[34] R.B. Taylor, B.J. Allen, A.R. de L. Musgrove, and R.L. Macklin, Aust. J. Phys. **32**, 551 (1979).

[35] J.H. Gibbons, R.L. Macklin, P.D. Miller, and J.H. Neiler, Phys. Rev. **122**, 182 (1961).

[36] M. Igashira, in *1995 Symp. on Nuclear Data*, Report JAERI-Conf 96-008 (Japan Atomic Energy Research Institute, Tokai-Mura 1996) p. 123.

[37] K. Wisshak, F. Voss, and F. Käppeler, Report FZKA–5968, Forschungszentrum Karlsruhe, 1997.

[38] R.F. Rose (Ed.),"ENDF–B Summary Documentation", report BNL–NCS–17541 4^{th}Ed (ENDF–BVI) Brookhaven Nat. Lab. 1991.

[39] Z. Y. Bao and F. Käppeler, Atomic Data Nucl. Data Tables **36**, 411 (1987).

[40] H. Beer, F. Voss, and R.R. Winters, Astrophys. J. Suppl. **80**, 403 (1992).

[41] Z. Y. Bao, private communications 1995.

[42] M.V. Bokhovko, V.N. Kononov, E.D. Poletaev, N.S. Rabotnov, and V.M. Timokhov, Proc. Int. Conf. on Nuclear Data for Science and Technology, Jülich, Germany, 1991 (Springer Berlin, Heidelberg, New York 1992) p.62.

[43] F. Käppeler, K.A. Toukan, M. Schumann, and A. Mengoni, Phys. Rev. C **53**, 1397 (1996).